PCCP

PAPER

View Article Online
View Journal | View Issue

Cite this: *Phys. Chem. Chem. Phys.*, 2017, **19**, 1190

"Energy Relay Center" for doped mechanoluminescence materials: a case study on Cu-doped and Mn-doped CaZnOS

Bolong Huang,*[a] Dengfeng Peng[b] and Caofeng Pan*[b]

Received 1st November 2016,
Accepted 22nd November 2016

DOI: 10.1039/c6cp07472c

www.rsc.org/pccp

We unraveled the mechanisms of transition metal-doped mechanoluminescent materials through a case study of CaZnOS. We found that the native point defect levels in Cu or Mn-doped CaZnOS system acted as energy relay centers for luminescence energy transfer. In combination with native point defect levels, discussed in a previous study [*Phys. Chem. Chem. Phys.*, 2016, **18**, 25946], we found that phosphor luminescence belongs to two different mechanisms. For Cu-doping, it occurs by the path *via* the conduction band minimum to the Cu-t_{2g} level of the 3d orbital localized in the band gap. The hole-drifting effect was found to support the reported red-shifting of the emission. Both reversible and irreversible mechanical quenching were attributed to the spatially separated electrons recombining with the hole localized on the Cu-t_{2g} level within the gap at levels below or above respectively. For Mn-doping, this occurs by a collaborative luminescence assisted by native point defects, and the excited states of Mn^{2+} overlap with the conduction band edge. The coexistence of Mn_{Zn} and Mn_{Ca} was confirmed, but was relatively low in Mn_{Ca}. The concentration quenching effect, as well as the red-shift of absorption, shows a strong correlation with native point defect levels and the relative position of the $4T_1(^4G)$ state for both Mn_{Zn} and Mn_{Ca}. Further simplified approximations were used for modeling such concentration quenching effects.

Introduction

In the recent decade, mechanoluminescence (ML) has shown great potential in energy conversion such as in applications for converting regular or irregular piezoelectricity, friction, and stress/pressure in nature.[1–6] The related materials have opened a wide range of channels for accommodating external excitations by UV (ultraviolet) photo-irradiation, near-infra-red (NIR, *e.g.* 980 nm) photo-stimulation, *etc.* The electron at the occupied trap level is excited to a higher energy state near the conduction band (CB) edge or inside the CB region, which is released backward to recombine with holes *via* either delocalized states in the CB or inter-level transitions within the optical band gap area of the host lattice. The energetic threshold for activating such electrons backward, using thermal perturbation or external mechano-stimulus, is relatively small in magnitude. The resulting visible luminescence for the electron–hole recombination at the activator site occurs by photon emissions.

To date, this class of luminescent materials has been well developed to a stage of both accurate and flexible properties modulations. Especially to excitation source, the external energy has been characterized in terms of physical variables like mechanical stimulation. The applications of ML materials are promising in fields of either large human infrastructure construction such as earthquake prediction, stability tests of large buildings or bridges, or in the area of electronics such as hand-input oriented multi-touch technology in a smartphone, or other mobile device in combination with magneto-optico-electronics.[7–9] More importantly, the demands in biological chemistry or biomedical areas urge such ML materials to have stronger intensities, longer lifetimes and lower costs with flexible wavelengths in persistent luminescence (phosphorescence).[10–20] The demands are particularly increasing currently in the fields of wound inspection in subcutaneous tissue, or human friendly *in vivo* or *in vitro* imaging studies for cancer tumor positioning or other related treatments.

However, as reviewed in ref. 12, 13 and 21, this technique of phosphorescence property-modulation stays in the pattern of experimental attempts through the combination of host materials and rare-earth (RE) based activating dopant ions.[22] Non-RE doping, such as transition metal or sp-block metal-assisted luminescence, is not systematically well explored and

[a] *Department of Applied Biology and Chemical Technology, The Hong Kong Polytechnic University, Hung Hom, Kowloon, Hong Kong SAR, China. E-mail: bhuang@polyu.edu.hk*
[b] *Beijing Institute of Nanoenergy and Nanosystems, Chinese Academy of Sciences, Beijing 100083, P. R. China. E-mail: cfpan@binn.cas.cn*

summarized. Moreover, the large promising area of "Biological Window" for *in vivo* imaging study of cancer tumor treatment is still missing or has unknown theoretical guidance for a mechanism study. An exact theoretical mechanism for persistent luminescence in terms of opto-electron excitation dynamics and charge carrier transfers is not clear. Moreover, the relationship between their native defect levels-assisted electron transport and their upconverted persistent luminescence property is also still far from being well understood, particularly at the electronic level. This lack of understanding not only hinders the process of designing new generations of persistent luminescence in the form of upconverted-mechano-persistent-luminescence (UMPL), but may also affect the further development of existing technology, such as "Inversed Design" for specific luminescence materials on-demand in various fields. Further investigations to fill the gap are of great significance in the relevant science and related technological applications.

Pan *et al.* have already shown a feasible technology to achieve RE-doped ML materials in both triboluminescence and phosphorescence through a smart combination with a single RE ion dopant.[3,6] This trend is heading toward a high color rendering character can be actualized by excitations of light-emitting-diode (LED) with Eu^{2+}-activator in ML materials.[23] This success arises because the well-known luminescence of f-block lanthanides has actually long been an important subject in optical applications and spectroscopic studies.[24–28] The lanthanide RE ions-assisted phosphorescence technique has aroused tremendous interests in biological, chemical and physical applications, and plays a leading role in modulating the luminescence properties.[29] From the previous work,[30] we also proposed the concept of the upconverted-mechano-persistent-luminescence (UMPL), which is based on long-decay-time phosphorescence.[12,13,21,31] The related application is challenged to downscale to smaller nano-sized particle synthesis with faster charge response, lower cost and longer time for luminescence or mechanical signal image.

This left a question of, besides the f-block lanthanides, whether the d-block elements like transition metal (TM) ions (*e.g.* Mn or Cu) also have rich and unknown theoretical stories behind the experimental manipulations of the ML intensity, color, and time-duration. Their mechano-stimulus, or doping concentration dependent ML, seems to also be a important topic for future prospective application or device manufacturing.[32] This confidence is sourced from the recent outcome reached by Xu *et al.*,[5,33] who demonstrated a substantial leap in this field because some ML materials, such as oxy-sulfides, can also be applied as persistent luminescence materials through transition metal doping and with flexible color manipulations,[34] especially particularly the "Biological Window" wavelength region. Such extended application not only requires our understanding on the electronic structures given by extrinsic doping, but also a high demand for plotting the photon–electron dynamic transitions based on the subtle energy conversion mechanisms during the process of persistent luminescence. Thus, to further the study of the phosphorescence of ML materials, herein, we focus on two typical transition metal ion (Cu and Mn) doping effects and take the host lattice CaZnOS as an example to illustrate the significance of native point defects-assisted collaborative phosphorescence.

However, the interplay effect of different point defect levels is a significant issue. As known from previous reports,[30,35–41] the native point defects in the host materials will not only produce a local lattice distortion or charge density anomalies, but also induce their unique localized electronic levels in the optical fundamental band gap either occupied or empty. In particular, ideally the lattice distortions among these defect reactions support the electron transfer between different optical transition levels with exact amounts of negative effective correlation energy ($-U_{\mathrm{eff}}$). The native complementary charged point defects form a time-accumulated donor–acceptor pair (DAP) and produce band-like levels within the optical band gap of host materials, which is pinned by the $-U_{\mathrm{eff}}$ effect along the closed cycle formed by zero-phonon-lines (ZPLs). Therefore, the stabilities and concentrations of native point defects from the host materials in persistent phosphor studies are quite important.

Another experimental difficulty is that thermally stimulated luminescence (thermal glow measurement, TSL) is used as an effective technology to measure the trap depth and impurity levels of the persistent luminescence materials. However, the TSL is carried out under a varied temperature condition that may modify the original native point defect levels of the host materials. This leads to the fact that the experimental observed trap level may not be the original trap level as we expected. Moreover, the emission peaks measured from TSL experiments are usually too broad, and form defect bands instead of levels that accurately influence the manipulation of luminescence. Thus, these exact inter-levels of activators and traps within the electronic structures suggested by the theoretical study will provide a reference for the selection towards the optimal performance.[30,35,36,42,43]

There have been some questions raised by pioneer experiments regarding the TM-doped CaZnOS: (I) for the Cu-doping study by Xu *et al.*,[5] they found a red-shift for the emission peak from the phosphorescence. Moreover, recoverable, unrecoverable, and enhanced mechanically induced quenching effects have been found systematically. This indicates the participation of the native point defects during the process of energy conversion for the luminescence. The Cu_{Zn}^{+} doping state has been induced for assistance of their schematic model. Thus, it is necessary to examine the single-particle levels of Cu substitutional doping in CaZnOS and subtle interplay between Cu doping level and native defect levels. (II) Differently, for the Mn-doping, Hintzen *et al.* have initially studied the Mn^{2+} doping in CaZnOS and obtained an efficient red luminescence with a single fixed peak centered at 614 nm.[44] They deduced that this red phosphorescence is actualized by Mn^{2+} optical transitions between the d–d transitions of Mn^{2+} itself in the lattice, and the crystal field effect also played an important contribution.[44] However, a detailed and systematically asymptotic doping behavior study updated the experimental observations and showed that the Mn^{2+} activated luminescence actually induces a red-shift of the phosphorescence, starting from about 607 nm to 625 nm, gradually increasing with Mn doping concentrations in CaZnOS.[34]

The absorption edge is also red-shifted with increased doping concentration by diffuse reflection spectra measurements. Furthermore, a 530 nm satellite emission was also found beside the 614 nm peak. Moreover, they found an Mn-doping concentration quenching effect, which was a uniform decreased behavior of brightness/intensity of phosphorescence, decay time, and optical band gap width, with increased Mn-doping concentration. This leads to a question that, if the luminescence only relies on the optical transitions between the d–d levels of $4T_1(^4G) \rightarrow 6A_1(^6S)$, why is there a concentration quenching effect? The optical band gap decreased with increasing doping amount of Mn, showing that it is also necessary to investigate the positions of $4T_1(^4G)$ level within the optical band gap. The X-ray diffraction (XRD) experiment on Mn-doped CaZnOS shows an evident shifting, leading us to question whether there is a coexistence of Zn and Ca substituted Mn doping in the host lattice. In addition, based on the discussion by Hochheimer *et al.*, there should have been a blue-shift effect among the transitions of $4T_1(^4G) \rightarrow 6A_1(^6S)$ instead of the as-discovered red-shift in Mn^{2+}-doped CaZnOS. Thus, crystal field effect is negligible or plays only a minor effect.

Proposed MQ modes by energy transfer

According to the abovementioned questions, in the present study, we interpret the phenomenon found in experiments based on previous calculation results and develop methods to interpret the questions raised from experiments of Cu-doping and Mn-doping induced luminescence. We think that these belong to two different mechanisms for phosphorescence in TM-doped CaZnOS. The as-discovered mechanical quenching effect will be discussed based on our calculated native point defect levels combined with Cu-doping levels.

As illustrated in Fig. 1, CaZnOS presents three possible mechanical quenching effects: reversible mechanical quenching (R-MQ), irreversible mechanical quenching (UR-MQ), and enhanced luminescence by mechanical quenching. For the ZnS system, there is a self-recoverable ML existing in ZnS, but disappears in ZnO due to the positions of different native point defect levels within the host band gap and acts in an assisting role for luminescence energy transfer.

In detail, the native electronic trap levels are accordingly divided by three classes. One is below the A-band (extra-deep donor trap levels), the second one is intermediated between the D- and A-bands, and the third is higher than the D-band. Herein, we proposed that the CaZnOS normally has three mechanical quenching effects: reversible mechanical quenching (R-MQ), irreversible-mechanical-quenching (UR-MQ), and enhanced effects. Based on the previous discussion, we know that the native point defects are widely separated within the band gap area. The donor (electron) and acceptor (hole) trap levels are ranged from shallow to deep positions. The D- and A-bands are the transition levels of luminescence centers, as discussed previously.

For the R-MQ, with loading applied, the first class electrons will be excited to the A-band to recombine the localized holes, forming a quenching effect. The luminescence intensity decreases. The previously excited electrons will turn backward to the original occupied levels because of the physical trend that the lower electronic level the more stability of electrons obtained in the band gap. Conversely, for the UR-MQ, the second class electrons move downward to recombine with the holes in the A-band with mechanical stimulation. When the stimulation takes off, the electrons would not fallback to the original levels as this is energetically unfavorable since they meet a backward energy barrier. The third class electronic levels are responsible for the enhanced effect. They can obtain enough high energy excitations to jump into the delocalized conduction band and

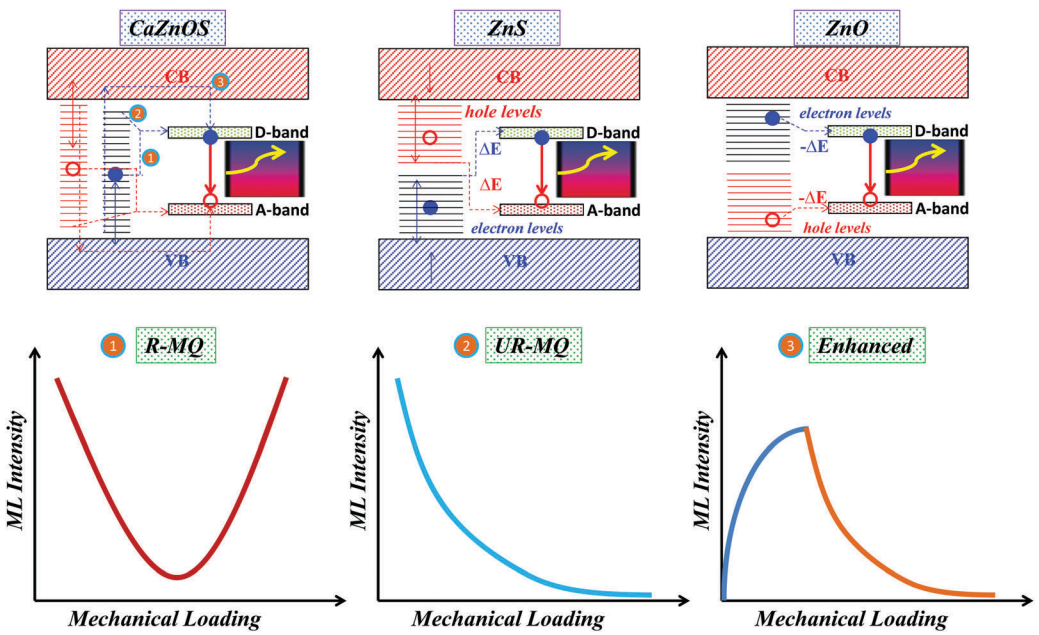

Fig. 1 Schematic for reversible and irreversible mechanical quenching (R-MQ and UR-MQ), as well as enhanced luminescence by mechanical loading.

transport to the D-bands accordingly. This process is equivalent to increasing the electron concentrations for recombination in terms of emitting photons between D- and A-bands.

For ZnS, the trap levels are mainly deep in the middle gap, as discussed.[45] Mainly, the second class type of traps, partially with the first class, was found to participate. The luminescence will decay in the form of UR-MQ when mechanical loading is the excitation source.

For ZnO, the electronic and hole levels are usually second class dominated, as calculated by one of our previous collaborators[46] and by Anderson and van de Walle.[47] Only a few of them will be excited by a substantial mechanical loading to the D-bands, whereas most of them will downshift to the A-band to quench the luminescence. Thus, with mechanical loading, the luminescence intensity will hardly improve, but decay quickly. Discussions are *vice versa* for hole-processes.

Calculation setup

For a better understanding of the electronic contributions of the Cu and Mn doping in CaZnOS, we have carried out first-principles calculations based on density functional theory (DFT) using the CASTEP code,[48] which basically inherited the calculation methods and setup used from the previous study.[30] We fixed the ground state relaxed lattice of CaZnOS geometrically, reported from our previous study, where the lattice constant we got was $a = b = 3.758$ Å, $c = 11.525$ Å, and $\alpha = \beta = 90^\circ$, $\gamma = 120^\circ$, within the $P6_3mc$ space group, which is the same symmetry as that of wurtzite ZnO.

For the plan-wave basis set, it is highly recommended to carefully extend the cutoff energy to 850 eV for describing the valence orbital components of Ca^{2+}, Zn^{2+}, Mn^{2+}, and $Cu^{2+/+}$ as well as the strongly localized states induced by the 2p orbitals of O^{2-} and 3p of S^{2-}. To guarantee convergence and avoid the charge-spin out-sync sloshing induced by the high-spin state of Mn^{2+} and Cu^{2+} (or Cu^{+}), we unanimously chose the ensemble DFT (EDFT) method of Marzari *et al.*[49] The convergence tolerance of total energy calculations was set not higher than 5.0×10^{-7} eV per atom, and the optimizations of Hellmann–Feynman forces in defect calculations were accomplished to lower than 0.01 eV $Å^{-1}$. The Baldereschi special *k*-point $(\frac{1}{4}, \frac{1}{4}, 0)$[50] with Gamma-center-off was self-consistently selected. Regarding the geometry relaxation, the algorithm based on the Broyden–Fletcher–Goldfarb–Shannon (BFGS) method was used through all bulk and defect supercell calculations.

The electronic density of states was simulated based on anisimov-type rotational invariant PBE+*U* calculations[51] since the PBE functional in DFT has been recognized to be reliable for structural relaxation and cell optimization of d or even f-orbital based solids,[52–54] regardless whether ultrasoft or norm-conserving pseudopotentials are present. Therefore, it is a suitable way to keep consistency by aligning with our previous study.[30] Furthermore, the rotational invariant *U* parameter has been self-consistently determined based on our previous methodology on the Hermitian type density matrix for both charge and potential diagonalization during the two-way cross-over perturbation. This method has demonstrated among oxides,[36,37,53–55] sulfides,[35] oxysulfides,[30] and fluorides[56] by our efforts and collaborations. Through our self-consistent determination process,[35–38,53–55] the on-site Hubbard *U* parameters for 3d of Ca and Zn are 2.50 eV and 13.45 eV, 2.87 eV for the 3p of S, and 3.44 eV for the 2p of the O. Moreover, the U_{3d} for Cu_{Zn} and Cu_{Ca} were self-consistently determined as 7.80 eV and 5.30 eV, respectively, while the vales were 3.46 eV and 2.70 eV for U_{3d} for Mn_{Zn} and Mn_{Ca} in CaZnOS, respectively.

It is worth addressing that, to reduce the influence of the localized hole states produced by the 2p orbitals of O sites and 3p of S sites, the self-consistently determined Hubbard *U* potentials were also applied on the O-2p orbitals and S-3p orbitals, which reached a consensus[57–60] in several oxides materials. Thus, it was necessary to consider both self-energy corrections on f- and p-orbitals for oxides.[37,38,55] By way of the OPIUM code in generation with the recent RRKJ optimization method,[61] we "tailor-made" the norm-conserving pseudopotentials within the most popular KB (Kleinman–Bylander) projector framework,[62] and the non-linear partial core corrections,[63] which had won recognition through our theoretical development.[37] Particularly for the pseudopotential of Cu, a valence configuration with ($3d^{10}$, $4s^1$) was chosen for representing the neutral Cu atom. This had been successfully used in our previous work for testing the deep hole trap levels induced by O-related native point defects states in a Cu_2O system with a corrected band gap, and showed good agreement with experimental observations.[53]

To calculate defect formation energy at different charge states (q), we consider that the overall supercell was established and remained constant based on the ground state relaxed primitive cell, to avoid the thermodynamic effect of enthalpy changes by cell variations. The formation energy of a targeted defect (H_q) at the specific charge state q can be described as a relation of the positions of Fermi energy (E_F) and the chemical potential ($\Delta\mu$) of defects α, which is shown as follows:

$$H_q(E_F, \mu) = \left[E_q - E_H\right] + q(E_V + \Delta E_F) + \sum_\alpha n_\alpha\left(\mu_\alpha^0 + \Delta\mu_\alpha\right), \quad (1)$$

The above E_q and E_H are the total energy of a relaxed defective lattice in charge state q and an ideal host lattice in the ground-state, respectively. The ΔE_F in eqn (4) is the change of Fermi energy with respect to the valence band maximum (VBM, $E_V = 0$), and n_α is the number of atoms of constituent element α chosen as the targeted defect site. μ_α^0 is the referenced chemical potential based on the method used in the study by Zunger *et al.*[64]

Results and discussion

Cu_{Zn} doping

Experimentally, two cation sites, Ca and Zn, are the possible center for Cu substitutional doping. Fig. 2(a) shows the partial density of states (PDOSs) of CaZnOS with Cu doped on Zn sites (Cu_{Zn}) at three different charge states, 0, +1, and +2. We can

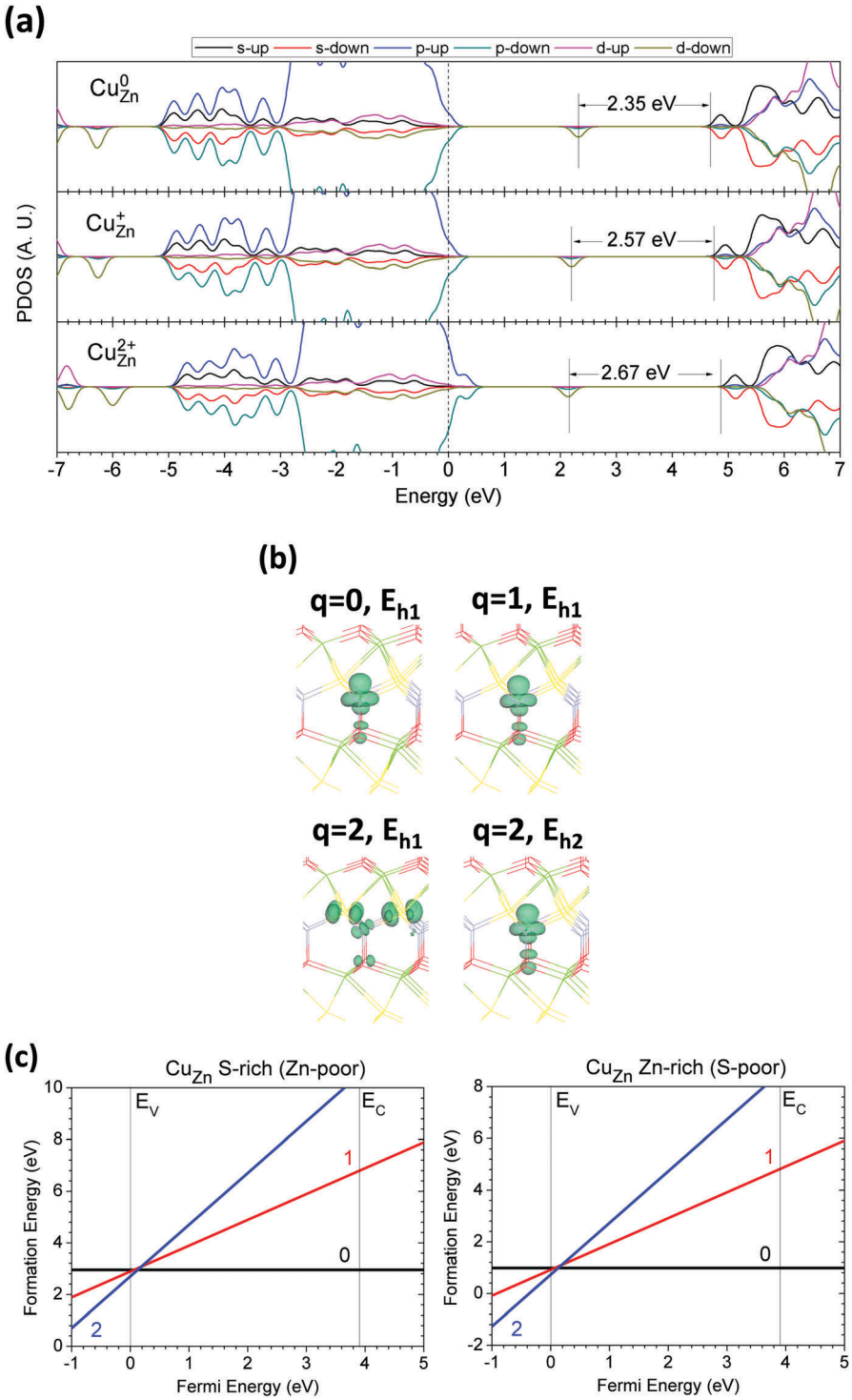

Fig. 2 (a) PDOSs of Cu_{Zn} in neutral (Cu^0_{Zn}), singly positive (Cu^+_{Zn}), and doubly positive (Cu^{2+}_{Zn}). The dashed line denotes the highest occupied level for electrons. (b) Localized electron and hole orbitals at the relaxed Cu_{Zn} site (Zn = gray, O = red, S = yellow, Ca = green, Cu = Brown). (c) Formation energies of Cu_{Zn} under S and Zn rich chemical potential limits.

treat it as [3S–Cu–O] for representing the local motif, and the Cu site is 4-fold coordinated in tetrahedral configuration. We see that Cu_{Zn} provides a deep hole trap center. As we can see, the localized defect levels are very different from the native V_{Zn} in CaZnOS from our previous study.[30] However, cation dopants with same ordinary charge states as the targeted substitution sites are usually the centers of localized hole traps and follow the previous observations based on a CaS system.[35] From the relaxed structure in the neutral state, the Cu^0_{Zn} induces less lattice relaxations compared to the native cation vacancy

defects, as discussed previously. The 3Cu–S bonds are 2.367 Å, 2.368 Å, and 2.376 Å, which are shortened by only 0.1–0.2 Å. The Cu–O bond has a length of 1.881 Å compared to 1.914 Å from the previous Zn–O bond. The PDOSs from Fig. 2(a) shows that the localized hole state of Cu^{0}_{Zn} is 2.35 eV below the CB edge in spin-down. There are a few electronic states that stay at the VB edge. For the Cu^{+}_{Zn} state, there are extra hole states pushed out from the top of the VB (VBM) in spin-down configuration, while the band tail-like electronic states remain at the VB edge. The Cu^{+}_{Zn} also gives a localized hole state 2.57 eV below the CB edge; this shows a close agreement with the observed phosphorescence emission wavelength of 483 nm (2.56 eV in photon energy) from the experiment carried out by Xu *et al.*[5] Further on the 2+ state (Cu^{2+}_{Zn}), the localized hole states turn out to be even shallower at 2.67 eV, far below the CB edge, and this also shows good agreement with results obtained with the experimental wavelength of 464 nm compared to experimental wavelength of 472 nm,[5] with only a relative deviation of 2%. In ordinary cases, the optical transitions between 3d–4s orbital levels are parity forbidden. However, as shown from Fig. 2(a), the CB edge consists of partially hybridized s and p orbitals that lower the restrictions of the selection rule. The optical transitions are, accordingly, allowed and this can be found in a similar statement from Tanner's study.[65] Therefore, the optical transitions between such a localized level and the CB edge are implementable and parity allowed.

Fig. 2(b) shows the orbitals for localized gap levels that were induced by the Cu_{Zn} in CaZnOS. We see that the localized hole states usually occupy hybridized $3d_{z^2}$ and $2p_z$ between the Cu and O sites, respectively, along the Cu–O bond direction. This scenario happens in three different charge states with different orbital expansion ranges in real space. In the +2 charge state (Cu^{2+}_{Zn}), an extra localized hole state is occupying the $3d_{xy}$ orbital and interacting with the localized $3p_{x,y}$ of the nearest neighboring S sites along the Cu–S bond direction. For the electronic states staying near the VB edge, as discussed above in Cu_{Zn}-doped CaZnOS, they are all found to be delocalized $3p_x$ or $3p_y$ orbitals and are wide spread in the lattice. This indicates that Cu_{Zn} will release the outer shell valence electrons into the Cu^{+}_{Zn} or Cu^{2+}_{Zn} state, which will enter the valence band as a stable state *versus* the Fermi level (E_F). The electrons will be spread over the in-plane $3p_x$ or $3p_y$ orbitals of S sites. We also see that the as-introduced localized hole state arises because of the correlations between partially occupied $3d^{10-\delta}$ ($0 < \delta < 1$) orbitals and 2p or 3p orbitals of O and S sites. There are no perturbed hole states (PHS) next to the CB edge.[66,67] The observed single localized hole level is different from the case of native point defect levels in other solid functional materials.[30,35–38]

The formation energy of Cu_{Zn} at 0, +1, and +2 is calculated and shown in Fig. 2(c). It shows that the Cu_{Zn} has a negative effective correlation energy (negative-U_{eff}) of −0.12 eV among the three different charge states. This indicates an exothermal defect reaction process of $2Cu^{+}_{Zn} \rightarrow Cu^{0}_{Zn} + Cu^{2+}_{Zn}$ and this is nearly ESR silent, or undetectable, in practical doping concentrations. The related negative-U_{eff} is obtained through the process: $U_{eff} = [E_{form}(q = 0) + E_{form}(q = +2)] - 2E_{form}(q = +1)$, where the formation energy is obtained from eqn (1) in the calculation setup. From the plot of formation energy *versus* the E_F, the negative-U_{eff} indicates that the crossover point between curves of neutral and doubly positive Cu^{0}_{Zn} and Cu^{2+}_{Zn} will be found under the curve of the singly positive Cu^{+}_{Zn} state.

Moreover, the concentration of Cu^{+}_{Zn} is relatively low compared to Cu^{0}_{Zn} and Cu^{2+}_{Zn}; however Cu^{+}_{Zn} it can be temporarily formed in the host with a short life-time by external UV photo-irradiation or other high-energy excitations. In order to further confirmation, we have tried the higher concentration Cu_{Zn} formation energy calculations within smaller CaZnOS supercell ($2 \times 2 \times 2$). The negative-U_{eff} turns out to be a more negative value of −0.25 eV, showing the physical chemistry trend that the low Cu^{+}_{Zn} concentration in CaZnOS is intrinsic. Therefore, our calculation shows that the discussed role of Cu^{+}_{Zn} in optical transition processes from the study by Xu *et al.* may be temporarily formed due to UV irradiation.[5]

Intrinsic formation of Cu^{+}_{Zn} in low concentrations contributes another possible route for optical transition or an energy relay center, as introduced by our previous study.[35] Such a Cu^{+}_{Zn} level is thermodynamically unstable and will experience the above-mentioned reaction transition into Cu^{0}_{Zn} or Cu^{2+}_{Zn}. In addition, the neutral Cu doping state (Cu^{0}_{Zn}) in CaZnOS has energies of 2.96 eV and 0.99 eV under the chemical potential of S-rich and Zn-rich limits, respectively. The thermodynamic transition level (TTL) of Cu_{Zn} is E_V + 0.125 eV for (0/2+) above the VBM (E_V for VBM). This implies that the Cu_{Zn} is an extra-deep donor-like trap center. The extra-deep donor level also indicates that the Cu^{0}_{Zn} will be the stable state in the band gap in a relatively wide E_F range from E_V + 0.125 eV (the TTL of (0/2+)) to E_V + 3.9 eV (CB edge). Therefore, the relative position of the TTL in the band gap for Cu_{Zn} is found to be in good agreement with the deduced schematic by Xu *et al.*;[5] however, according to our calculations, it was found to be the transitions of (0/2+).

Cu_{Ca} doping

We turn to look at Cu_{Ca} doping in the CaZnOS lattice, which is [3O–Cu–3S] as the local motif and 6-fold coordinated in a distorted A7-like local structural configuration. As indicated in Fig. 3(a), the PDOSs show a trend similar to the case of Cu_{Zn}. Among the three different charge states, 0, +1, and +2, the localized hole states are all deep in the band gap of the host lattice, as well as some electronic and hole band tail states at the VB edge near the E_F. In the relaxed neutral Cu_{Ca}-doped structure, the Cu–O bond was shortened from 2.354 Å to 2.042 Å, while the Cu–S bond was elongated to 3.223 Å compared to the original Zn–O and Ca–S bond lengths in CaZnOS. The PDOSs from Fig. 3(a) shows the localized hole state of Cu^{0}_{Ca} is 2.64 eV (470 nm) above the VBM, in close consistency with the experimental wavelength of 472 nm,[5] and some shallow acceptor-like states are at the top of the VB acting as the VB band tail. For the Cu^{+}_{Ca} doping state, the hole-like VB band tail states turn out to be more evident as 0.20 eV in difference compared to the spin-up state. The energy interval between the localized mid-gap hole state and the VB tail is 2.93 eV. For Cu^{2+}_{Ca}, the localized hole state is 2.58 eV (481 nm) higher than the hole-like VB tail state (0.33 eV above the E_F), which is also close to the experimental wavelength of 483 nm.[5]

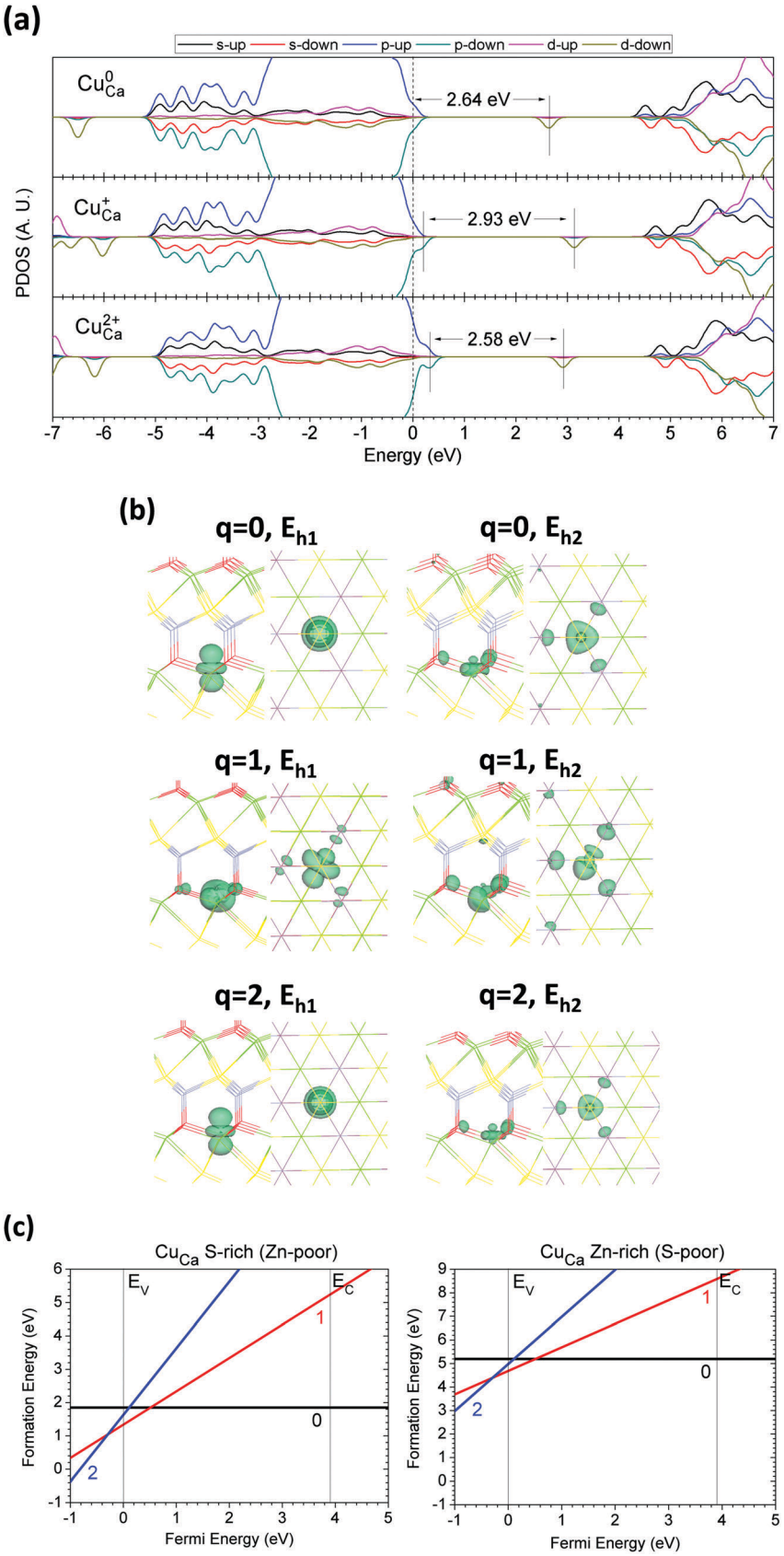

Fig. 3 (a) PDOSs of Cu_{Ca} in neutral (Cu^0_{Ca}), singly positive (Cu^+_{Ca}), and doubly positive (Cu^{2+}_{Ca}). The dashed line denotes the highest occupied level for electrons. (b) Localized electron and hole orbitals at the relaxed Cu_{Ca} site (Zn = gray, O = red, S = yellow, Ca = green, Cu = Brown). (c) Formation energies of Cu_{Ca} under S and Zn rich chemical potential limits.

Based on the as-discussed localized hole levels of Cu_{Ca}, the optical transition paths that match the experimental emission wavelength in phosphorescence are different from the case of Cu_{Zn} in CaZnOS. In the Cu_{Ca} doping case, the optical transition is from the localized mid-gap hole to the VB tail state, while for Cu_{Zn}, it is from the CB edge to mid-gap hole state.

As indicated in Fig. 3(b), the orbitals of the localized levels induced by Cu_{Ca} are slightly different from the Cu_{Zn} in CaZnOS. This difference can also be found from our self-consistently determined on-site Coulomb potential Hubbard parameter for Cu (5.298 eV for Cu_{Ca} and 7.805 eV for Cu_{Zn}). In the Cu^0_{Ca} state, the deep localized hole state shows a single isolated $3d_{z^2}$ orbital from the Cu dopant site. This indicates a potential weak interaction for Cu in 6-fold coordination [3S–Cu–3O] by substituting into the original Ca site. Another localized hole state stays at the CB edge with p–d orbital hybridization between Cu and three S sites in the plane of the CaS sub-lattice of the CaZnOS system. For the Cu^+_{Ca} state, the localized hole orbitals are evidently different from the neutral state. The localized mid-gap hole state is anisotropic and in the $3d_{z^2}$ component configuration, horizontally coupling with the nearest neighboring O sites in the CaO sub-lattice layer. Moreover, the other is near the CB edge with more evident hybridization between the 3d and 2p orbitals of Cu and O, respectively. The localized hole state orbitals in Cu^{2+}_{Ca} are rather similar to the neutral state with a smaller range for the isosurface of orbitals in real-space, denoting less localized holes nearby.

Fig. 3(c) shows the calculated formation energy of Cu_{Ca} at charge states of 0, +1, and +2. We see that the Cu_{Ca} requires more energy to be doped than Cu_{Zn}. This may be because Cu has a more similar ionic radius to Zn compared to Ca in the CaZnOS host lattice. This denotes that the Cu_{Ca} in CaZnOS possesses positive effective correlation energy (positive-U_{eff}) with a value of +0.81 eV for the defect reaction process of $2Cu^+_{Ca} \rightarrow Cu^0_{Ca} + Cu^{2+}_{Ca}$. It indicates an endothermal process for such a reaction and Cu^+_{Ca} is supposed to be the dominant Ca substitutional doping state in the CaZnOS system. The TTL of the state (0/+) is E_V + 0.51 eV above the VBM (*i.e.* E_V for VBM), and the TTL of the state (+/2+) is $E_V - 0.30$ eV below the VBM. From the formation energy *versus* the E_F, the Cu^0_{Ca} is the relatively stable doping state within most of the E_F range of the gap above the E_V + 0.51 eV. The neutral doping state of Cu_{Ca} in CaZnOS has a formation energy of 5.20 eV and 1.85 eV under the chemical potential of S-rich and Zn-rich limits, respectively. The formation energy of Cu^+_{Ca} is estimated to be 4.69 eV and 1.34 eV under the S-rich and Zn-rich limits, respectively. As discussed above, the relative position of the TTL (0/+) in the band gap for Cu_{Ca} is obtained to be the position near the VB edge, which is in good agreement with the energy diagram by Xu *et al.*[5] However, the formation energy of Cu_{Ca} is obviously higher than Cu_{Zn} in CaZnOS, more than 2 eV in energetic magnitude.

Mn_{Zn} doping

We turn to the case of Mn doping on substituting the Zn site from CaZnOS, which is a potential application for red-luminescence with an emission wavelength of ~610 nm experimentally.[33,34]

From the partial density of states targeted on the Mn doping site, for the neutral state (Mn^0_{Zn}), we found there are a few extra deep donor levels from their single-particle level in the PDOS (Fig. 4(a)). Their localized electronic levels stay at E_V + 0.096 eV, E_V + 0.263 eV, and E_V + 0.358 eV above the VBM (E_V denotes the VBM). The localized hole levels are contributed by the Mn 3d-fine levels in the spin-down configuration, with E_V + 4.578 eV, E_V + 4.604 eV, E_V + 4.679 eV, E_V + 4.726 eV, E_V + 4.906 eV, and E_V + 4.977 eV respectively, buried into the conduction band region of the host CaZnOS. The energy interval between the lowest hole level and highest electronic level is 4.578 eV, which is far beyond the emission photon energy (~2.03 eV) of experimentally reported luminescence (~610 nm).[33,34] Thus, we deduced that the emission photon energy may not be sourced from the direct de-excitation from the excited Mn level to the ground state level correspondingly.

For the Mn^+_{Zn} doping state, the localized electronic levels stay at E_V + 0.071 eV, E_V + 0.154 eV, and E_V + 0.193 eV above the VBM, whereas the localized hole levels are distributed in two regions near the band gap. One part is at the VB edge with spin-up as a shallow hole level, the other is spin-down at the CB edge and consisting of fine levels of localized hole states as nearly deep acceptor bands (Fig. 4(a)). The spin-up shallow hole level is E_V + 0.460 eV higher than the VBM in the gap. The spin-down deep hole bands are distributed into five fine levels with energetic intervals of about 0.05–0.2 eV. They are E_V + 4.224 eV, E_V + 4.313 eV, E_V + 4.375 eV, E_V + 4.558 eV, and E_V + 4.661 eV, respectively, residing in the conduction band in a uniform trend aligned with the case of Mn^0_{Zn}. Similarly, the minimum energy interval between spin-up electronic and spin-down hole levels is 4.031 eV, and slightly wider than the Mn^0_{Zn} state. The minimum interval between the spin-up and spin-down hole level is 3.764 eV, close to the magnitude of the optical fundamental band gap of the host CaZnOS.

For the Mn^{2+}_{Zn} doping in CaZnOS (Fig. 4(a)), there are two localized electronic levels that stay at E_V + 0.032 eV and E_V + 0.146 eV above the VBM acting as deep donor states, while the localized hole levels show a behavior similar to the case of Mn^+_{Zn}. There are two spin-up shallow hole levels that stay at E_V + 0.322 eV and E_V + 0.419 eV above the VBM in the gap. For the spin-down deep hole levels, they are present as fine-levels with very small energetic intervals below the conduction band minimum (CBM). Moreover, such fine-levels consist of a hole band that overlaps with the CB edge, partially in the delocalized CB region and the rest falls into the band gap area below the CBM. The relative positions of such fine-levels are given as E_V + 3.668 eV, E_V + 3.835 eV, E_V + 3.897 eV, E_V + 4.031 eV, and E_V + 4.121 eV. The energy interval between the above higher spin-up hole level and the lowest spin-down hole level is 3.249 eV, while 3.522 eV is for the interval between the highest electronic level and the lowest spin-down hole level.

From the abovementioned analysis, the native luminescence for electrons de-excitation for Mn in three different charge states is not the direct contributing source of the ~610 nm luminescence.

Fig. 4(b) shows the orbitals of the localized electrons and holes levels induced by Mn_{Zn} in CaZnOS. The neutral doping

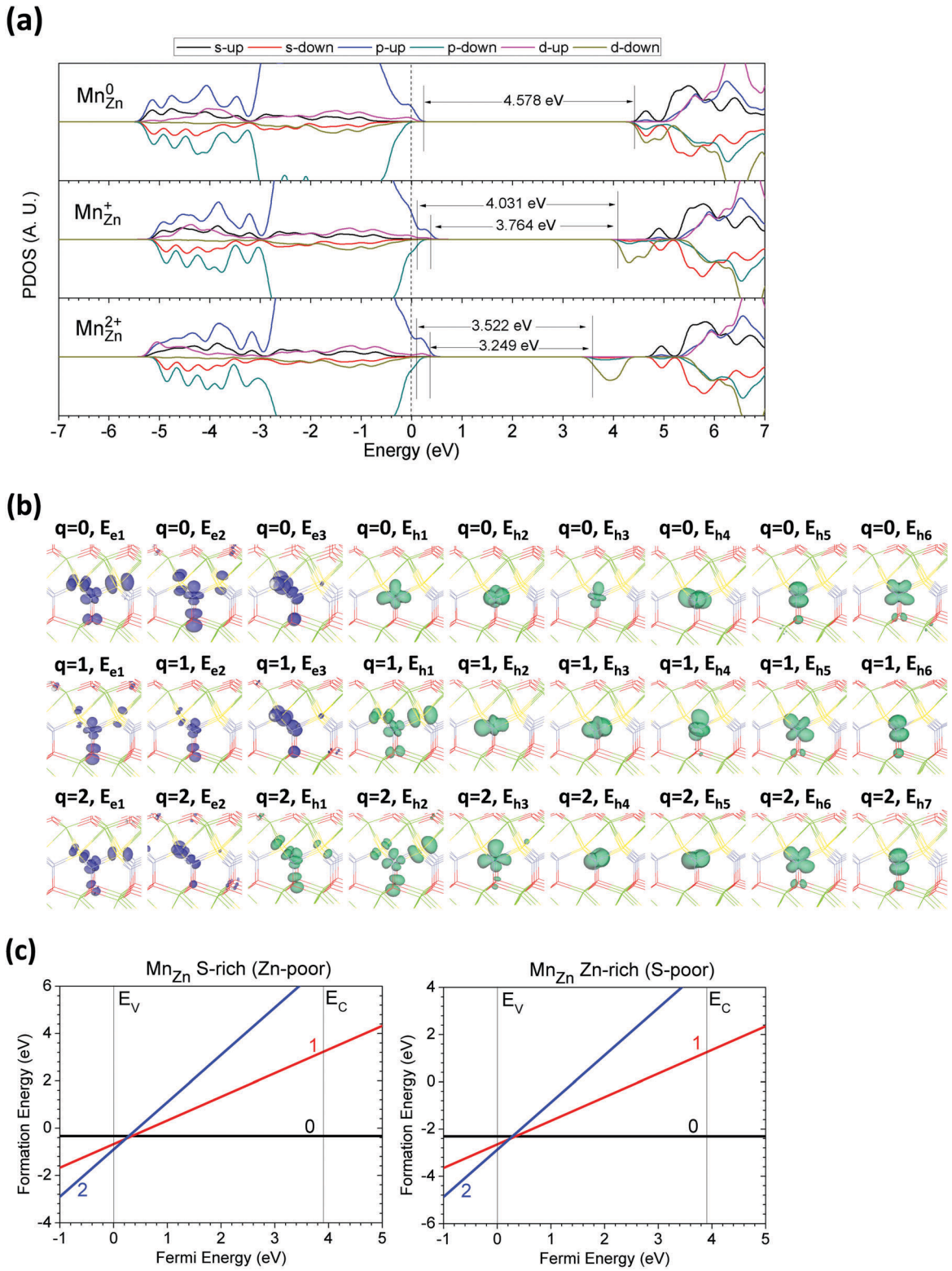

Fig. 4 (a) PDOSs of Mn_{Zn} in neutral (Mn^0_{Zn}), singly positive (Mn^+_{Zn}), and doubly positive (Mn^{2+}_{Zn}). The dashed line denotes the highest occupied level for electrons. (b) Localized electron and hole orbitals at the relaxed Mn_{Zn} site (Zn = gray, O = red, S = yellow, Ca = green, Cu = Brown). (c) Formation energies of Mn_{Zn} under S and Zn rich chemical potential limits.

state shows that the electronic levels have an evident p–d orbital coupling effect between three Mn_{Zn}–S and Mn_{Zn}–O bonds. The Mn shows a $3d_{z^2}$ and orbital feature and also a linear combination of $3d_{xy}$ and $3d_{xz}$ components for the third electronic

state next to the VBM. The hole fine-levels given by the Mn_{Zn} in the neutral state show isolated 3d orbitals with different components or combinations, with an energy band width of 0.393 eV. In the Mn_{Zn}^{+} state, one of the hole levels turns down to the level where it is near the electronic state. Due to the electron–hole Coulomb attractive effect, the orbital of such a state keeps the p–d coupling feature localizing between Mn_{Zn}–S and Mn_{Zn}–O bonds. In the Mn_{Zn}^{2+} doping state, the hole levels near the VBM show a similar p–d coupling effect around the local structure of [3S–Mn_{Zn}–O].

The formation energies of Mn_{Zn} at 0, +1, and +2 charge states are indicated in Fig. 4(c). The trend in physical chemistry shows that the neutral formation energy is more energetically favorable compared to the Mn_{Zn} doping. A similar effect has also been found from our previous study in the CaS system with Eu and Dy doping.[35] It also indicates a positive-U_{eff} for the Mn_{Zn} in CaZnOS, experiencing a charge transition from the defect reaction process: $2Mn_{Zn}^{+} \rightarrow Mn_{Zn}^{0} + Mn_{Zn}^{2+}$, with a value of +0.11 eV. This means the concentration of Mn doping sites in the singly positive charge state may be higher than the one at Mn_{Zn}^{0} or Mn_{Zn}^{2+}. The TTL of the (0/+) state is E_V + 0.34 eV above the VBM and the TTL of the state (+/2+) is E_V + 0.23 eV above the VBM. From the E_F dependent formation energy, the Mn_{Zn}^{0} is stable in most areas of the band gap from E_V + 0.34 to E_C = 3.90 eV (CBM). The neutral formation energy is −0.33 eV and −2.31 eV for Mn doping at the Zn site in CaZnOS, under chemical potential of S-rich and Zn-rich limits, respectively. The reason for the negative formation energy is analyzed in two different ways. One, it shows a physical chemistry trend that the Mn_{Zn} doping is energetically favorable as Mn has a very similar ionic radius to Zn in CaZnOS. Another reason is the formation energy *versus* the E_F calculation by DFT is performed under 0 K conditions. If we extrapolate the related chemical potential terms in Gibbs free energy $\Delta G = \mu_0 + \mu(p,T)$ for the formation of Mn_{Zn}, we may obtain the positive formation energy under ambient conditions (300 K, RT) or at even higher temperatures during the synthesis process. Therefore, such a formation energy calculation can be a good reference when compared to other doping species at the Zn site such as abovementioned Cu_{Zn}, *i.e.*, Mn_{Zn} is more dopable than Cu_{Zn}.

Mn_{Ca} doping

We turn to look at the case where Mn substitutes the Ca site in CaZnOS. The PDOSs of the Mn_{Ca} are shown in Fig. 5(a) with 0, +1, and +2 charge states. For the Mn_{Ca}^{0} doping state, there are two localized electronic levels with E_V + 0.162 eV and E_V + 0.206 eV above the VBM in the spin-up direction. The localized holes are similarly distributed at the fine-levels inside the CB region, which are E_V + 4.592 eV, E_V + 4.917 eV, E_V + 5.115 eV, E_V + 5.181 eV, and E_V + 5.206 eV, respectively, with an all spin-down configuration. The minimum energy interval between the electron and hole levels are 4.386 eV, which has already exceeded the optical fundamental band gap limit (3.90 eV).

For the singly positive state (Mn_{Ca}^{+}), there also shows two spin-up electronic levels localized above the VBM with E_V + 0.153 eV and E_V + 0.213 eV. One of the hole states shifts into the gap with E_V + 0.522 eV above the VBM with spin-up. The other holes are all spin-down and distributed at the unoccupied fine-levels starting from the CB edge to the regions inside the CB, which are E_V + 3.891 eV, E_V + 4.044 eV, E_V + 4.197 eV, E_V + 4.347 eV, and E_V + 4.481 eV, respectively. Similarly, it is relatively large for the minimum energy interval between the electron and hole levels, which is 3.678 eV. While for the interval between spin-up and spin-down hole levels, it is 3.582 eV.

For the Mn_{Ca}^{2+}, there are no localized electronic states induced by Mn_{Ca} at charge state +2. All of the localized states are unoccupied and act as hole levels in two parts in the gap. One part is spin-up with E_V + 0.302 eV and E_V + 0.400 eV above the VBM in the gap. The other part is spin-down and almost evenly distributed as fine-levels for holes or excited electrons induced at the Mn_{Ca}^{2+} site. This part with fine-levels is actually different from the other two states, Mn_{Ca}^{0} and Mn_{Ca}^{+}, since the levels are all well below the CB edge in the optical fundamental band gap region. The levels are E_V + 3.243 eV, E_V + 3.284 eV, E_V + 3.328 eV, E_V + 3.459 eV, and E_V + 3.465 eV, respectively. The minimum energetic interval between spin-up and spin-down hole levels is 2.843 eV.

The localized orbitals of the corresponding electronic and hole levels in the gap are shown in Fig. 5(b). For the neutral doping state (Mn_{Ca}^{0}), the orbitals of the electronic levels near the VB show an interaction among 3d of Mn, 2p of O and 3p of S sites. The $3d_{xy}$ type orbital component is presented on the Mn site for larger overlapping with the adjacent p orbitals of nearby S and O sites. For the deep acceptor levels, as seen inside the CB, all of the orbitals are isolated on the Mn sites with either single or combined d orbital combinations. For the Mn_{Ca}^{+} state, the orbital distribution for the electronic state appears to be weaker than the one in the neutral state (Mn_{Ca}^{0}). It indicates that the ionized electrons in the excited state are not purely sourced from the Mn doping site; in fact, they may be provided from the unity of charge density distributed around the local structural motif of [3S–Mn–3O]. One of the holes stays near the VB with a strong p–d coupling effect near the S–Mn–O local area. The other five localized orbitals are the five representative fine-levels of holes given by the Mn at the excited state, located at the position overlapping with the CB edge. For the Mn_{Ca}^{2+}, all of the localized orbitals represent the hole levels as there are no electrons localized. These include the hole levels sitting near the VBM with spin-up and hole fine-levels that are well below the CBM, given by Mn^{2+}.

Fig. 5(c) shows the DFT-calculated formation energy at the three charge states, 0, +1, and +2, for Mn_{Ca} in CaZnOS. It seems to be a doping center with negative-U_{eff}, with a value of −0.07 eV. This shows that the defect reaction process for $2Mn_{Ca}^{+} \rightarrow Mn_{Ca}^{0} + Mn_{Ca}^{2+}$ could be easily affected by external conditions, and is capable of being either an exothermal or endothermal process since the $|U_{eff}|$ is too small. The neutral formation energy of the Mn_{Ca} is 0.49 eV and −2.86 eV under the chemical potential limits of S-rich and Zn-rich at 0 K, respectively. Considering Mn_{Zn}^{0} at S-rich limit, its formation energy was found to be −0.33 eV estimated at 0 K by DFT. This evident energetic contrast, accordingly, implies that the Mn_{Zn} is

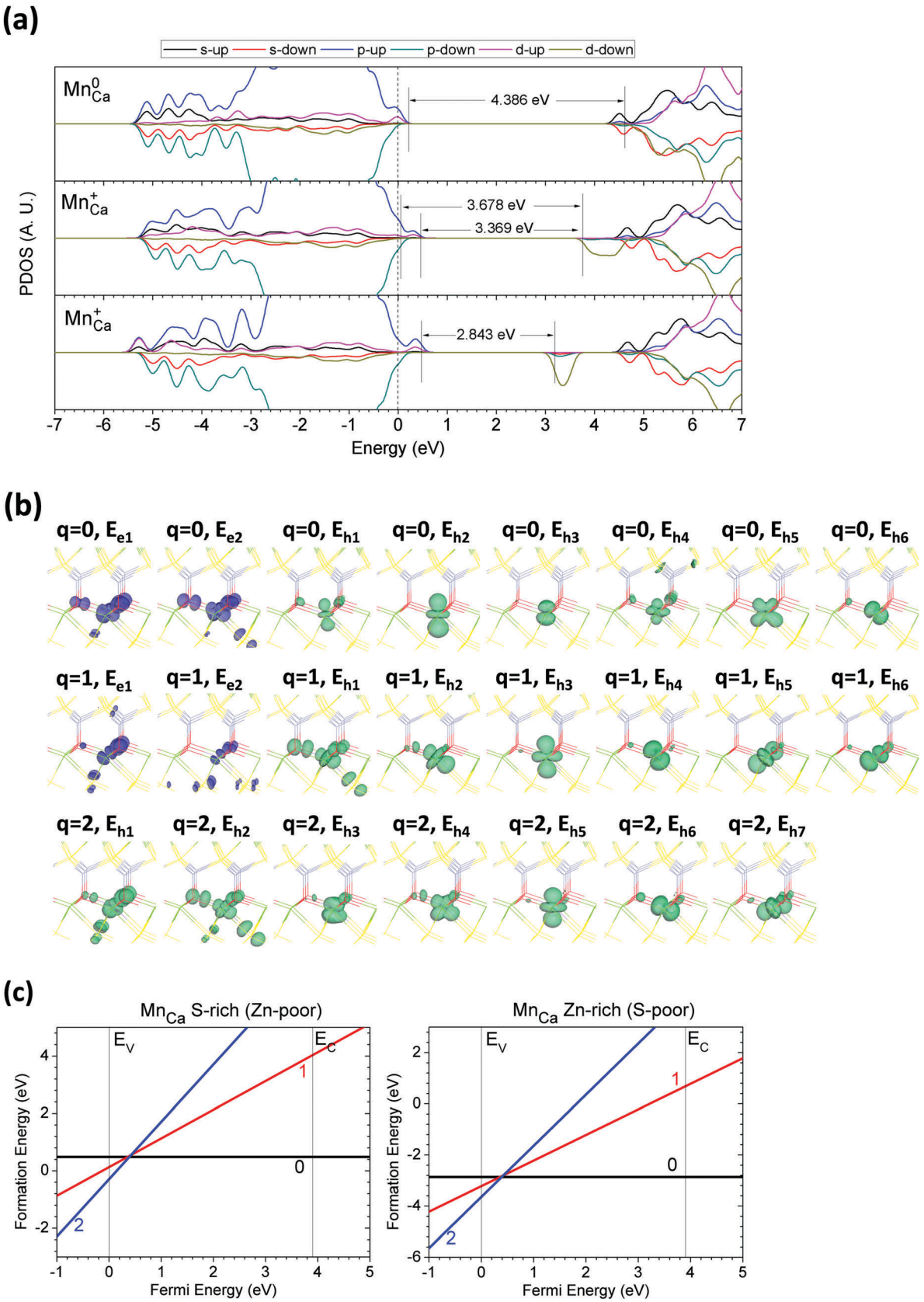

Fig. 5 (a) PDOSs of Mn_{Ca} in neutral (Mn^0_{Ca}), singly positive (Mn^+_{Ca}), and doubly positive (Mn^{2+}_{Ca}). The dashed line denotes the highest occupied level for electrons. (b) Localized electron and hole orbitals at the relaxed Mn_{Ca} site (Zn = gray, O = red, S = yellow, Ca = green, Cu = Brown). (c) Formation energies of Mn_{Ca} under S and Zn rich chemical potential limits.

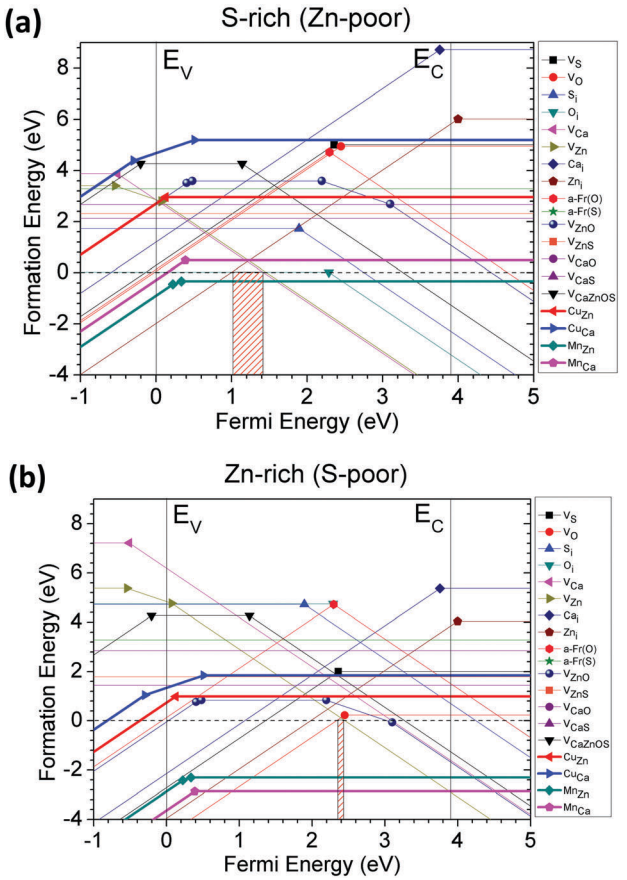

Fig. 6 Summary of the native point defects in CaZnOS under S-rich (a) and Zn-rich (b) chemical potential limits, with considerations from Cu (Cu_{Zn} and Cu_{Ca}) and Mn (Mn_{Zn} and Mn_{Ca}) doping. Orange shaded area denotes the dopable range for tuning the E_F positions that would not cause the spontaneous formation of native point defects or opposite charges for compensation.

found to be more easily doped than Mn_{Ca}. The TTL of the state (0/2+) on Mn_{Ca} site is 0.28 eV above the VBM, showing a deep donor like dopant in the CaZnOS system, in a similar range provided for Mn_{Zn}.

Energy levels in luminescence

Dopants and photo-generated native point defects

Before the discussion on luminescence mechanism, we need to look at the doping limit for the CaZnOS determined by the native point defect levels. As shown from our previous study on the CaS system, we illustrate that the dopable range is actually determined by the lowest formation energy defects, in which the external doping would not cause spontaneous formation of oppositely charged defects in the host.[35] Herein, as indicated in Fig. 6(a) and (b), we combined all the discussed native point defects at different charge states from the previous study,[30] with the currently considered Cu_{Zn}, Cu_{Ca}, Mn_{Zn} and Mn_{Ca} at the charges of 0, +1, and +2, under the chemical potential limits of S-rich and Zn-rich.

From Fig. 6(a), in the S-rich limit, the dopable range represented by the E_F position is from E_V + 1.015 eV to E_V + 1.422 eV, as shown in orange shaded area. This arises because Zn_i^{2+} and V_{Zn}^{2-} in the band gap area through most of the E_F region are the lowest formation energy defects. This behavior is different from the findings in the previous studied CaS system,[35] indicating that CaZnOS is totally different from CaS. Therefore, some subtle interplays between the Mn_{Zn} and V_{Zn}^{2-} or Zn_i^{2+}, as the Zn site is the easiest substitution site for Mn to be doped in CaZnOS, have been shown. Moreover, the Mn_{Zn} shows the lowest formation energy behavior near the dopable range, but the V_{Zn}^{2-} and Zn_i^{2+} surpass the Mn_{Zn} to be the lowest energy defects in the rest of E_F range within the band gap region. Therefore, Mn_{Zn} doping in the system would have a large possibility of causing the formation of V_{Zn} or Zn_i nearby. While the detail charge states may vary from those discussed above, the physical chemistry trend in Gibbs free energy model remains rigid.

For Cu doping, it costs more energy than Mn does. Moreover, the Cu_{Zn} is evidently lower than the Cu_{Ca} throughout the E_F range of the band gap. Furthermore, below the TTL of (0/2+), the formation energy diagram of V_{ZnO}^{2+} almost merges with Cu_{Zn}^{2+}. This means that below the TTL of (0/2+) for Cu_{Zn}, the V_{ZnO}^{2+} and Cu_{Zn}^{2+} are energetically un-separated, *i.e.*, the V_{ZnO}^{2+} and Cu_{Zn}^{2+} are energetically equivalent and are formed in CaZnOS with equivalent possibility. Accordingly, the V_{ZnO}^{2+} may act as an intermediate level for transfer of the holes from Cu_{Zn}^{2+} so as to transfer/forward the original activator (sensitizer) site (Cu_{Zn}^{2+}) to a new designated activator site (V_{ZnO}^{2+}). We have gained related experience through our previous study in cubic Cu_2O where the deep hole trap levels are found through two types of intrinsic defects.[53] Moreover, we also found that the formation energy level of V_{CaZnOS}^{0} shows relatively higher than the level of Cu_{Zn}^{0} at the 0 and +2 charge state, but turns to be lower starting from E_V + 2.0 eV at the charge state of −2. These clues promoted us to further investigate, through the discussion, the single-particle levels of dopants and native point defects in CaZnOS in a clearer picture.

Fig. 6(b) shows the native point defects formed under Zn-rich limits. The dopable range gets narrower than the case found in Fig. 5(a). Differently, in the CaS system, the dopable ranges in Ca-rich and S-rich limits have equivalent energy widths in E_F within band gap area. However, in CaZnOS, the chemical potential limits are supposed to consider four different cases with difficulties in calculation. With consideration of experimental data,[68] the S-rich and Zn-rich limits are mostly covering the experimental synthesis conditions, of course, with some extent of imperfections. This would not affect us to discuss the doping formation energy levels of Cu and Mn in CaZnOS. We found the formation energy level of Cu_{Zn} is obviously above the V_{ZnO} formation diagram. Both the Mn_{Zn} and Mn_{Ca} are well below all the native point defect energy levels, and the Mn_{Ca} doping turns out to be the lowest formation energy under the Zn-rich potential limit. Therefore, even under the metallic element rich potential limits for synthesis conditions of the CaZnOS system, the formation of Cu and Mn substitution doping will certainly cause formation of some native point defects from the host lattice. This will provide a solid reference for our further investigations on the mechanism of luminescence found in Cu-doped[5] and Mn-doped systems.[33,34]

Another highlight worth mentioning is that, though the photo-irradiation usually takes the bound electrons from the top of the VB to the CB for the host lattice, it is also an external source of energy transferred into the host, resulting in a generation of native point defects. We may call it photo-generated native point defects for understanding the subtle interplay between native defect levels and photo-sensitizer typed dopants. In addition, as we know, experimental photo-excitation wavelengths have been reported in the range from 280 nm[34] to 304 nm,[44] which is about the range from 4.08 eV to 4.43 eV in photon energy. The above high energy photo-irradiation has indeed reached the energy levels that can generate most of the native point defects from the host lattice, as shown from either Fig. 6(a) or (b).

Inter-transitions between single-particle levels

a. Luminescence induced by Cu substitution doping. Fig. 6(a) shows that the doping sites such as Cu_{Zn} and Cu_{Ca} generally have higher energy than most native point defects, and Cu_{Ca} has a higher cost energy to form than Cu_{Zn}. This energy difference is about 2.2 eV high. Therefore, it is reasonable to consider the electronic properties contributed by Cu_{Zn} only.

We combined the single particle levels of native point defects with Cu_{Zn} and Cu_{Ca} for the charge states of 0, +1, and

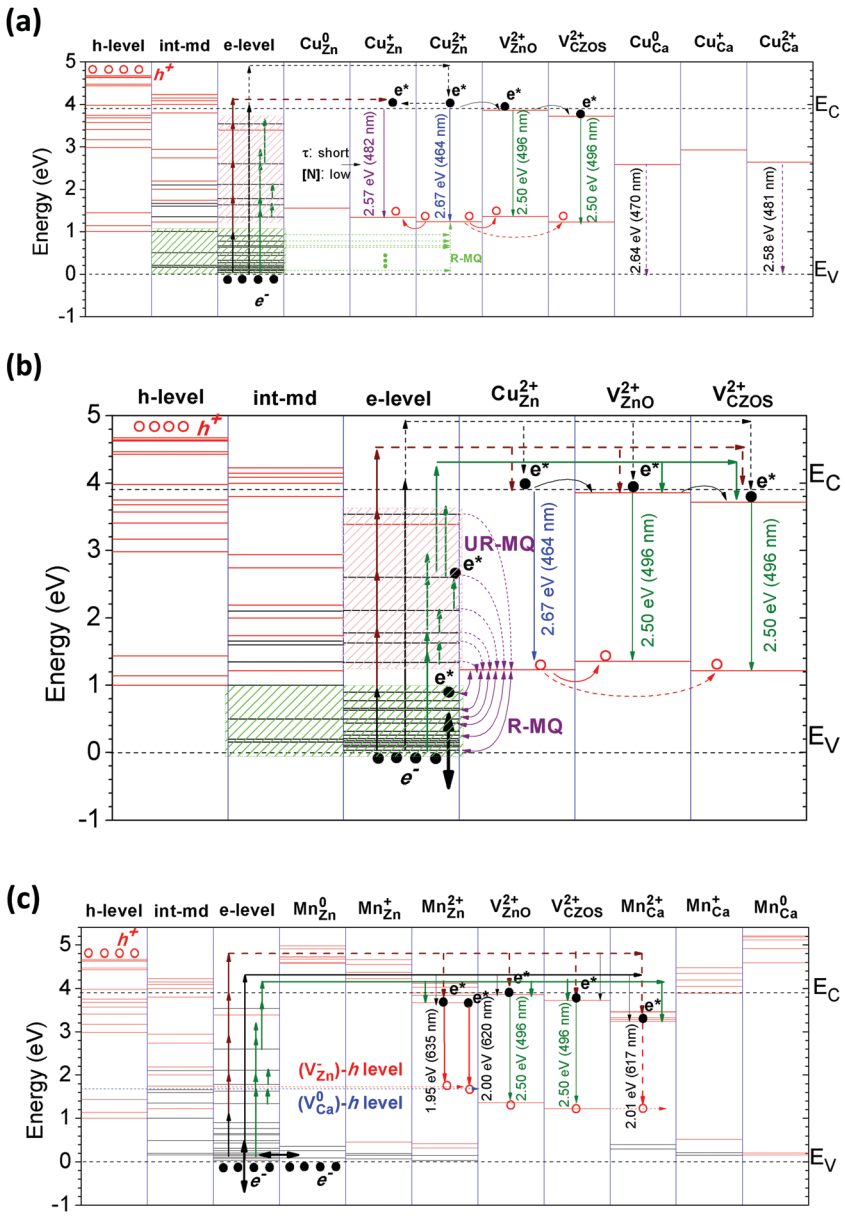

Fig. 7 (a) Summarized single-particle levels of intrinsic defects in CaZnOS with different charge states (empty states = red, filled states = black) and the related Cu_{Zn} and Cu_{Ca} doping levels. (b) Summarized energy diagram for illustrating the mechanism of R-MQ and UR-MQ effects of the Cu-doped luminescence process. (c) Summarized single-particle levels of intrinsic defects in CaZnOS with different charge states (empty states = red, filled states = black) and the related Mn_{Zn} and Mn_{Ca} doping levels.

+2, as indicated in Fig. 7(a). As discussed in the above section, the Cu_{Zn} doping produced deep hole trap levels near the mid-gap area with 2.57 eV and 2.67 eV below the CBM for Cu^{+}_{Zn} and Cu^{2+}_{Zn}, respectively. The Cu^{0}_{Ca} and Cu^{2+}_{Ca} contribute to the electronic de-excitation paths with energy intervals of 2.64 eV and 2.58 eV, respectively. However, the formation energy of Cu^{0}_{Ca} is too high throughout the optical band gap area, even for the Cu^{2+}_{Ca} within the VB area under the S-rich limit. Basically, the optical transitions between s and d orbitals are parity forbidden by selection rules. However, as seen from the PDOS analysis, the CBM consists of partially hybridized s and p orbitals. This will increase the probability of the optical inter-band transition or give rise to higher optical oscillator strength as the p → d optical transition is allowed.

As illustrated in the Fig. 7(a), external energy excitation approaches 980 nm near-infra-red (NIR), UV irradiation, and mechano-stimulus, by the vertical dark brown, black, and green arrows respectively. In particular for the green vertical line, different scales of mechano-stimulus have been shown and can effectively pump-up electrons gradually from the localized electronic trap levels to a higher state near the CBM or the CB region. With initial UV-irradiation (365 nm, *i.e.* 3.40 eV) by experiments,[5] the electrons at the Cu^{0}_{Zn} doping site are easily excited into a higher state and are ionized into the CB range by a small energetic threshold.

We then looked at the role of Cu^{+}_{Zn}. As we discussed above, the Cu_{Zn} is a negative-U_{eff} center where Cu^{+}_{Zn} exists in the host lattice (CaZnOS) in a low concentration or with a short life-time. This doping state can also act as a luminescence activator center by emitting 2.57 eV photons or 482 nm in wavelength. As the life-time for electron occupation on this level is short, it will be further transferred to another state for luminescence, which is the V^{2+}_{ZnO} since they are energetically equivalent, as discussed in previous section (Fig. 6(a)). This has further confirmed, slightly modified, and enriched the proposed mechanism from the experiments of Xu *et al.*,[5] and the data are in agreement with the experimental report.[5]

Thus, the trend is as follows: (1) $Cu^{0}_{Zn} \rightarrow Cu^{2+}_{Zn}$ by external high-energy UV irradiation; (2) $Cu^{2+}_{Zn} \rightarrow Cu^{+}_{Zn}$ by capture of the electrons de-excited from the CBM at Cu^{2+}_{Zn} site; (3) $2Cu^{+}_{Zn} \rightarrow Cu^{0}_{Zn} + Cu^{2+}_{Zn}$ by the negative-U_{eff} effect; and (4) $h(Cu^{2+}_{Zn}) \rightarrow h(V^{2+}_{ZnO})$ by the hole drifting effect it can be said that, higher the localized hole levels, more the stability the hole reaches, and also the formation energy diagram of Cu^{2+}_{Zn} and V^{2+}_{ZnO} are merged as energetically equivalent. By process (2), the luminescence wavelength is shifted from 464 nm (2.67 eV) to 482 nm (2.57 eV) in a short time, consistent with the experimentally reported red-shift from 472 nm (2.63 eV) to 483 nm (2.57 eV) within the time-duration of 1 min. Due to the increased amount of Cu^{+}_{Zn} given by process (2), the negative-U_{eff} effect will drive process (3) and the electrons will be transferred by a non-radiative process, which may take 5 min in transition as indicated by the experiments of Xu *et al.*[5] Process (4) will be furthered by the driving force of lower Gibbs free energy represented by the formation energy calculations. The Cu^{2+}_{Zn} and V^{2+}_{ZnO} are energetically equivalent, and a significant hole-drifting takes effect due to the lower energy level for holes to transport towards V^{2+}_{ZnO} (shown by red curved arrow in Fig. 7(a)). After process (4), the photo-sensitizer center is transferred to the V^{2+}_{ZnO} site and the emission peak of phosphorescence is stabilized at 496 nm (2.50 eV) after 20 min, as shown in experiment.[5]

Another interesting experimental observation that is necessary to be considered in our calculation is the mechanical quenching. Xu *et al.* observed both reversible and irreversible mechanical quenching effects (R-MQ and UR-MQ) during the phosphorescence at 472 nm for Cu-doped CaZnOS.[5]

We elucidated the small energetic scaled mechano-stimulated electron–hole recombination in Fig. 7(b). This is a simplified diagram to draw-out the paths of how electrons recombine with holes non-radiatively for quenching the photon-emission at the activator sites. This arises because of two factors: one is that the Cu_{Zn} formation energy is at a higher cost than most native point defects. Another factor is that, the existence of Cu_{Zn} usually comes with some native point defect levels, as shown in Fig. 6(a). Thus, it is necessary to combine the contributions of electronic levels given by the native point defect levels with the localized hole level of Cu^{2+}_{Zn}.

As summarized from our previous study,[30] for instance, V^{0}_{Zn}, V^{-}_{Zn}, V^{2-}_{Zn}, S^{0}_{i}, and O^{0}_{i} induce localized electronic levels above the VBM and below the localized hole levels of Cu^{2+}_{Zn}. The V^{0}_{ZnO}, V^{-}_{ZnO}, V^{0}_{O}, V^{-}_{CaZnOS}, V^{2-}_{CaZnOS}, a-Fr^{0}_{O}, and a-Fr^{+}_{O} have crossover ranges for formation energies and can provide electronic levels slightly higher than the hole level of Cu^{2+}_{Zn}. The O^{2-}_{i}, a-Fr^{-}_{O}, and a-Fr^{2-}_{O} can provide both higher and lower energies than the hole level of Cu^{2+}_{Zn}. Xu *et al.* have also proposed that the V_{Zn} is one of the defects responsible for the MQ effect,[5] and it acts as a deep non-radiative center. From our calculations, we further confirmed their analysis and also classified the different contributions by V_{Zn} within different charge states in detail. The V_{Zn} in all charge states (0, +1, and +2) are found to be the R-MQ center.

It is also interesting to note that the UR-MQ centers contributed by the native point defects above are also responsible for enhancing the phosphorescence intensity when external mechano-stimulus is loaded on the sample after 12 h.[5] This arises because such a long enough time-duration indicates that all the Cu^{2+}_{Zn} turns back to the Cu^{0}_{Zn} state, or transfers the activator center to the V^{2+}_{ZnO} or V^{2+}_{CaZnOS} sites by the process (4) summarized above. With the increase of the loaded mechano-stimulus, the trapped electrons in the filled state are subsequently excited to the higher states near the CBM or at the CB edge. These mechano-excited electrons (as indicated by green arrows) will de-excited back and recombine with the holes at the V^{2+}_{ZnO} or V^{2+}_{CaZnOS} sites. The higher the load of external mechano-stimulus, the more electrons are promoted to the excited level near the CB edge. Therefore, the phosphorescence intensity will be increased accordingly.

Another thing is the consideration of the defects with very low formation energy. In particular for O_i, as shown in Fig. 6(a) and the discussion we provide previously, it has very low formation energy that is rather close to the zero formation energy level. Therefore, it is almost a free mobile state in the

S-rich chemical potential limits. According to the electronic levels that are localized near the VBM or deep in the gap by O_i^0 and O_i^{2-}, such a type of defect (O_i) is the phosphorescence "killer" by mechanical-stimulus. As the ionic radius of O_i^{2-} is small enough to across the host lattice, the sample powder of as-synthesized CaZnOS exposure in the air under the ambient conditions are very easily absorbing the O_2 molecules or $O_2^{\delta-}$ ($0 < \delta < 2$) and they are dissolved into the lattice with forms of O atoms or ions respectively. This process will generate large O_i throughout the host CaZnOS lattice, playing the role of mobile MQ center carrying opposite charges. Moreover, it has a formation energy lower than Cu_{Zn} and needs external mechano-stimulus to promote its level to be energetically equivalent to the Cu_{Zn} state.

We schematically classified and summarized the R-MQ and UR-MQ energetic regions for phosphorescence by Cu_{Zn}^{2+} in CaZnOS. As indicated in Fig. 7(b), the solid curved violet arrow denotes the R-MQ process. Electrons occupying the localized levels below the E_V + 1.2 eV of Cu_{Zn}^{2+} in the band gap are capable of being excited to recombine with the holes staying on such a level, while these electrons will be easily de-excited backward to the originally occupied levels as the lower the electronic level, the more stable to the electrons in the band gap. Conversely, the dashed curved violet arrow denotes the UR-MQ process. The electrons will be activated with a small energetic threshold to drop into the hole state that is 1.2 eV above the VBM non-radiatively. These electrons will hardly come back to the original occupied energy levels. Because these levels are higher than the level of E_V + 1.2 eV, and it turns out to be a backward energy barrier for electrons.

b. Luminescence induced by Mn substitution doping. We turn to look at the case of Mn doping in CaZnOS. The Mn^{2+}-activated CaZnOS was first systematically studied by Duan and Hintzen,[44] whose experiments show that a phosphor emission ranged from 550 nm (2.25 eV in photon energy) to 700 nm (1.77 eV in photon energy) and can be assigned into the transition between $4T_1(^4G) \rightarrow 6A_1(^6S)$. A more recent study shows an extensively detailed characterization of phosphorescence and a red-shift of the luminescence. The amount of luminescence related properties are dependent on the Mn^{2+} doping concentrations.[33,34]

From Fig. 6, the energy difference between Zn and Ca substituted Mn doping is about 0.82 eV with Mn_{Zn} and forms 0.33 eV below the zero formation energy and only 0.49 eV above the zero energy level for Mn_{Ca}. Therefore, they are both relatively easy to be doped in CaZnOS while Mn_{Zn} exists in a slightly higher concentration. On the other hand, this can be understood as the scenario where, in the process of a Mn-doping concentration dependent experiment, the Mn will firstly occupy the Zn site and then the Ca site with the dosage of Mn doping gradually increasing. Therefore, the Mn doping from low to high concentration is actually a process from the substitution of Zn-sites (Mn_{Zn}) to the Ca-sites (Mn_{Ca}).

Moreover, in Fig. 7(c), we have shown that the Mn-doped CaZnOS contains 3d fine-levels that stay above the CB, at the CB edge, and below the CB or overlapped, for the charge states of 0, +1, and +2, respectively. This is also consistent for both Mn_{Zn} and Mn_{Ca}. The energy band width for the 3d fine-levels near the CB shows about 0.5 eV in average for Mn_{Zn} with small differences, while the width given by the Mn_{Ca} is 0.3–0.7 eV (0.3 eV for charge state q = 0, 0.5 eV for q = +1, and 0.7 eV for q = +2). Two experiments conducted at different time-stages both showed the absorption band width from the $4T_1(^4G)$ to $4T_2(^4D)$ in the corresponding energy of 0.67 eV at the maximum.[34,44] This is given by the energy difference from the absorption peaks of $4T_1(^4G)$ ($\sim$510 nm, *i.e.* 2.43 eV) and $4T_2(^4D)$ ($\sim$400 nm, *i.e.* 3.10 eV), respectively.[34,44] Our calculated band width shows good agreement with the experimental observations, and denotes the possible coexistence of Mn_{Zn} and Mn_{Ca}.

Fig. 7(c) shows the paths of luminescence by electron–hole recombination. The dark brown, black, and green arrows vertically denote the different manner of external excitations on electrons, such as 980 nm near-infra-red (NIR), 200–300 nm UV irradiation, and mechano/tribo-stimulus in the local lattice with piezo-electrical energy, respectively. Moreover, the oppositely charged holes are correspondingly excited in the same manner and are located at the localized hole states in the optical band gap or near the VB/CB edge. This process is called spatial charge separation by native point defects, as illustrated in our previous study, Fig. 1 of ref. 30; the external energy was then subsequently harvested at such localized levels. The excited electrons, denoted as "e*" in Fig. 7(c), will fall back to the lower energy levels and recombine the excited holes to release energies through photon emissions at the specific levels.

We further noted that the Mn_{Zn} doping sites distributed among the host lattice are actually seen as Mn occupying the intrinsic V_{Zn} sites in CaZnOS that are natively formed during the synthesis process. Thus, the single-particle levels between them are correlated to some extent. The localized hole state at E_V + 1.7 eV is given by the V_{Zn}^- calculated previously,[30] and also shown in Fig. 7(c), while such a state is not relatively stable compared to Mn_{Zn} according to the formation energy calculation under the S-rich (or Zn-poor for Zn deficit, *i.e.* for V_{Zn}) limit. It will capture an additional electron to form V_{Zn}^{2-}, and hence, stay below the Mn_{Zn}^0 formation energy diagram (Fig. 6(a)) reaching an even more stable state than Mn_{Zn} through the band gap area. The trapped de-excited electron will consequently be transferred back to the levels that were close to the VB edge or inside of VB region, which were originally excited from the VB or levels near the VB edge.

From Fig. 7(c), the higher shallow localized hole level induced by Mn_{Zn}^{2+} occupies above the VBM at E_V + 0.42 eV. Based on this level, we also found another phosphorescence path from the localized electronic level of V_{ZnO}^- to the E_V + 0.42 eV, which represents the electron moving towards a lower energy where the hole stays. From Fig. 6(a), the formation energy of V_{ZnO}^- *versus* the E_F within the band gap is not relatively stable compared to the Mn_{Zn}^0 and Mn_{Zn}^{2+}; thus, the electrons that are occupying the V_{ZnO}^- sites will be transferred towards the localized shallow hole levels provided by Mn_{Zn}^{2+} in the band gap, and release the energy in the form of photon emissions. The photon energy is about 2.1 eV, consistent with experimentally observed emission peak position of 2.02 eV (614 nm). Thus, there are two proposed

paths for Mn_{Zn}^{2+} induced phosphorescence. One is from $4T_1(^4G)$ of Mn_{Zn}^{2+} to the V_{Zn}^{-}, while the other is from V_{ZnO}^{-} to the $6A_1(^6S)$ of Mn_{Zn}^{2+}.

Experimentally, it has been also reported another evident phosphor luminescence with emission peak at about 530 nm (*i.e.* 2.34 eV in photon energy) but in a lower intensity.[34] For the analysis on experimental peak levels, we interpret them from the single-particle levels calculation results reported previously, the V_{ZnO}^{2+} is a suitable site that carries the excited electrons to attract them within a short life-time passing through the localized hole levels to recombine the holes occupying at the lower level (E_V + 1.35 eV). The V_{CaZnOS} shows similar behavior as discussed previously, but at an even higher energy cost to transport the electrons between Mn_{Zn}^{2+} and V_{CaZnOS}^{2+} under S-rich chemical potentials. Therefore, V_{ZnO}^{2+} is the only suitable native point defect level for collaborative phosphorescence to contribute to the experimentally reported 530 nm emission. Our calculated energy interval for such optical inter-level transition was 2.32 eV (*i.e.* 534 nm in wavelength), in good consistency to experimental observations.[34] Due to the relatively high energy cost of V_{ZnO}^{2+} compared to Mn_{Zn}^{2+} in CaZnOS, the charge carrier recombination activity between these two sites becomes a minority. The optical emission intensity is lower compared to the dominant 614 nm emission.[33,34,44]

Fig. 7(c) also shows that the hole level given by V_{Ca}^{0} from the host lattice also seems to be a suitable level that merges with $4T_1(^4G)$ of Mn^{2+} to form a combined activator site. Under the S-rich limit, this was also confirmed from the formation energy diagram that, above the TTL of state (2−/−) for V_{Zn}, the energy diagram of V_{Ca}^{2-} and V_{Zn}^{2-} are almost merged and act as energetically equivalent sites for such a combined activator center of Mn^{2+} doped phosphorescence in CaZnOS. While for the potential Zn-rich limit, the V_{Ca}^{2-} almost overlaps with the energy diagram of V_{ZnO}^{2-}. Thus, we deduced that the V_{Ca}, V_{Zn}, and V_O sites are mutually interacting under an unknown mechanism, which will be explored in a future work.

Now for the Mn_{Ca}^{2+} state, the transition width between $4T_1(^4G) \rightarrow 6A_1(^6S)$, was found to be 2.84 eV in the CaZnOS system. The optical transition between these two states is too wide to match the experimentally observed 614 nm phosphorescence. Formation energy calculations show that the Schottky type V_{CaZnOS} defect can be formed below the formation energy of Mn_{Ca} doping within the band gap area shown in Fig. 6(a), and the related energy diagram is also close to the V_{Ca} even under the metallic rich potential limit (Fig. 6(b)). Based on our previous single-particle level calculations on native point defects, the V_{CaZnOS} has two localized hole states within the band gap area, with one about 0.2 eV below the CBM, and the other E_V + 1.23 eV above the VBM.[30] From the TDOS calculation on Mn_{Ca}^{2+}, the lowest excited state $4T_1(^4G)$ sits below the CBM, which is E_V + 3.24 eV (E_V for VBM); therefore, the optical inter-level transitions between this energy interval will release the energy in the form of photons of about 2.01 eV (or 617 nm), in close agreement with the experimentally observed phosphorescence peak centered at 614 nm.[33,34,44]

c. Concentration quenching effect by Mn doping. The original experiment done by Hintzen *et al.* has shown that the Mn^{2+} in CaZnOS activated an efficient red luminescence with a single peak fixed at 614 nm, regardless of the doping concentration variation effect.[44] Further detailed work presented a red-shift of the peak with movement of 12 nm, representing a photon energy difference of 0.04 eV.[34] As with our analysis above, this arises because the localized hole levels that accommodate the de-excited electrons drift from V_{Zn}^{-} to V_{Ca}^{0} through a spatial charge transportation or tunneling effect if these two defects stay within a close distance. Also, according to Fig. 7(c), our calculated single-particle levels show that the energetic difference of these two localized hole levels is 0.05 eV, which is from 620 nm to 635 nm (red-shift of 15 nm), in good agreement with the experimental value (within an acceptable error magnitude). Why does this happen? This arises because, the holes drift from the original V_{Ca}^{0} site onto the V_{Zn}^{-} site, and Fig. 6(a) also confirms that the V_{Zn}^{-} has lower energy than V_{Ca}^{0} near the VBM. The free holes will drift from the original V_{Ca} to the V_{Zn} site and photon energy emission (*via* the inter-level transitions) is red-shifted to a lower energy.

Another interesting effect reported experimentally is summarized into the concentration quenching effect. First of all, the optical band gap decreases with increased amounts of Mn doping due to the red-shift of the photo-absorption edge. From the above analysis together with Fig. 6(c), we see that the $4T_1(^4G)$ levels were all below the CBM for the Mn_{Zn}^{2+} and Mn_{Ca}^{2+} doping states, while the one in Mn_{Ca}^{2+} presents lower (E_V + 3.243 eV) than the Mn_{Zn}^{2+} (E_V + 3.668 eV). We used a relative position fraction to represent them as the $4T_1(^4G)$ level of Mn_{Zn}^{2+} occupies 6% of the E_g (E_g denotes the band gap of the host, 3.90 eV by our calculation) below the CBM, while 17% of the E_g for Mn_{Ca}^{2+}. Compared with the experiment, it is found that 6% of the E_g for Mn_{Zn}^{2+}, while 11% for Mn_{Ca}^{2+},[34] shows good consistency between our calculations and experimental observations.

As indicated in Fig. 8(a), after the doping, the measured optical band gap by photo-absorption spectroscopy was attributed to the optical vertical transitions of VB $\rightarrow$ $4T_1(^4G)$ of Mn^{2+}. We have discussed the coexistence of Mn_{Zn} and Mn_{Ca} in the previous section as their formation energy difference is only 0.8 eV with the zero energy line in the middle. Thus, in a small amount of Mn-doping, Mn_{Zn} is the dominant doping site. While with increased Mn-doping concentrations, the Mn_{Ca} becomes more and more evident in occupation from the view of thermal equilibrium statistics. Thus, the $4T_1(^4G)$ of Mn_{Ca}^{2+} shifts downwards to a deep range away from the CBM, leading to decreased optical vertical transition intervals. This is the reason that the experimental measured optical band gap is decreased with Mn-doping concentration increased.[34]

The experiment further found the Mn-doping concentration quenching effect, which is a uniformed decrease behavior of brightness/intensity of phosphorescence, decay time, and optical band gap width, with increases in the Mn-doping concentration. This leads to a question that, if the luminescence only relies on the optical transitions between d–d levels of $4T_1(^4G) \rightarrow 6A_1(^6S)$, why will it have a concentration quenching effect? As a discussion on the optical band gap width dependent on Mn doping concentrations, we deduced that

the quenching effect was also attributed to the occurrence of Mn_{Ca}, as its neutral formation was also rather low (about 0.3 eV under the S-rich limit). The emission spectra of the host lattice observed from photoluminescence (PL), tribo-ML, compress-ML, and ultrasonic-ML and cathodoluminescence (CL) all present a typical peak doping composition of $x = 0.003$–0.004. This aroused our attention and further interest to carry out a simple approximated model to illustrate the significant role on the co-existence of Mn_{Ca} in the lattice.

First of all, we assumed the occupations of V_{Zn} and V_{Ca} were a and b (a,$b > 0$). Considering the thermo-equilibrium statistical effect, the rate of Mn occupying the V_{Zn} to form Mn_{Zn} was η_1 and η_2 (η_1,$\eta_2 > 0$) for the case of occupying the V_{Ca} to form Mn_{Ca}. The total doping composition of Mn into the lattice of CaZnOS after thermal equilibrium was shown to be x ($x > 0$).

For the stage of very low dosage of doping, we approximated Mn_{Zn} as the dominant doping state and Mn_{Ca} as negligible, which means:

$$\begin{cases} 0 \le \eta_1 x \le a - \eta_1 x \\ 0 \le \eta_2 x \ll b \\ \eta_2 x \to 0 \end{cases} \quad (2)$$

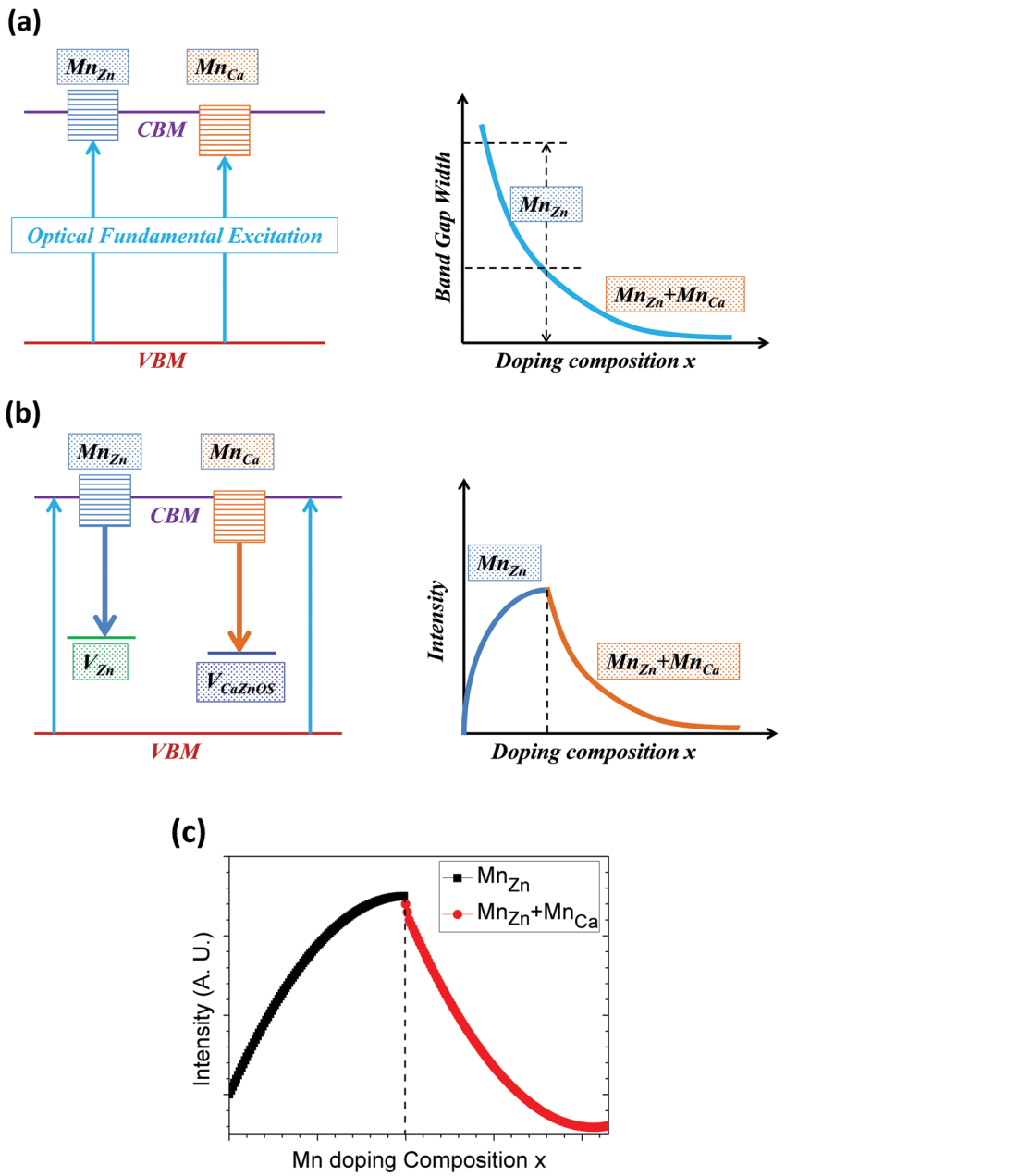

Fig. 8 (a) Schematic illustrating the band gap width dependent on the Mn doping concentration due to the absorption edge being red-shifted. (b) Schematic diagram with analysis model to demonstrate the Mn-doping concentration quenching effect. (c) Numerical fitting model to model the diagram in (b).

The intensity represented by I, is yielded within the range as follows:

$$0 \le I = \min[(a-\eta_1 x)\eta_1 x] \le \frac{a^2}{4} \quad (3)$$

With increased doping concentrations of Mn, the occupation on V_{Ca} for Mn_{Ca} doping becomes more evident. We consider this to be the intermediate range to match the fact that the experimental x was not very large. The intensity is represented as follows:

$$\begin{cases} a-\eta_1 x \le \eta_1 x \\ 0 \le \eta_2 x \le b-\eta_2 x \\ I = I_{Zn} + I_{Ca} = (a-\eta_1 x)^2 + (b-\eta_2 x)\eta_2 x \end{cases} \quad (4)$$

With this analysis, we plotted the relationship between I and x based on eqn (3) and (4), shown in Fig. 8(b) and (c). The plot contains two parabolic-curves with two different opening directions. The peak center is shown as $x = \frac{a}{2\eta_1}$, which is also the turning point between these two different parabolic-curves. Experimental spectra show the uniformed turning-x at the peak, it is consistently shown by us that the turning point at $x = \frac{a}{2\eta_1}$ is an intrinsic value that represents the properties of the host lattice.

We finally see the formation energy in the S-rich limit. The Mn_{Zn} and Mn_{Ca} are both in an energetically favorable E_F range within the optical band gap. All of the related native point defects form with relatively higher energy than Mn doping. Accordingly, in the opinion of formation energy, it further tells us that the related luminescence shall be dominantly considered at the Mn_{Zn} and Mn_{Ca} induced localized levels within the band gap. This also follows a trend of physical chemistry in chemical potentials for electronic transport. Therefore, the previously discussed native photo-activator sites, such as V_{ZnO} and V_{CaZnOS} with 2.50 eV energy intervals, are not the dominant sites of charge carrier recombination for phosphorescence. The excited electrons will first come through the levels induced by Mn^{2+} sites and recombine with the holes at the levels selected by the formation energy, as discussed above.

Conclusion

In summary, motivated by novel discoveries from pioneers and experts,[5,34] we have discussed the transition metal doped CaZnOS with a case study of the Cu-doped and Mn-doped systems. The interplay effect of native point defects is rather significant as an energy relay center among the process of mechanoluminescence. We illustrated that the combinations of native point defects and doping levels yielded two interesting mechanisms in the two doped systems. The energy transfer in luminescence passes *via* CBM to the Cu-t_{2g} level of the Cu-3d orbital localized within the band gap in the Cu-doped system. The red-shift effect is interpreted by a hole-drifting effect within the band gap. Both reversible and irreversible mechanical quenching (R-MQ and UR-MQ) effects are attributed to the spatially separated electrons that recombine with the hole localized on Cu-t_{2g} level within the gap, with levels below or above respectively. We have also found an intriguing energy conversion mechanism in the Mn-doped case, which is native point defects participated collaborated phosphor luminescence. The 3d fine levels of the Mn^{2+} doping state overlap with the CBM, and the $4T_1(^4G)$ state is below the CBM. The formation energy calculations confirmed the coexistence of Mn_{Zn} and Mn_{Ca}, but the existence is relatively low in Mn_{Ca}. This is key to explain the Mn doping concentration quenching effect as well as the red-shift of the absorption edge. We attached to such findings with a simplified approximation and elucidated an intrinsic property of Mn-doped CaZnOS to present a concentration quenching effect.

Acknowledgements

The author BH gratefully acknowledges the support of the Natural Science Foundation of China (NSFC) for the Youth Scientist grant (Grant No. NSFC 11504309), the initial start-up grant support from the Department General Research Fund (Dept. GRF) from ABCT in the Hong Kong Polytechnic University (PolyU), and the Early Career Scheme (ECS) fund (Grant No. PolyU 253026/16P) from the Research Grant Council (RGC) in Hong Kong. This work is supported by the high performance supercomputer (ATOM-project) in Dept. of ABCT of PolyU.

References

1 Z. L. Wang, *Nano Today*, 2010, **5**, 540.
2 W. Wu and Z. L. Wang, *Nat. Rev. Mater.*, 2016, 16031.
3 X. Wang, *et al.*, *Adv. Mater.*, 2015, **27**, 2324.
4 D. Peng, B. Chen and F. Wang, *ChemPlusChem*, 2015, **80**, 1209.
5 D. Tu, C.-N. Xu, Y. Fujio and A. Yoshida, *Light: Sci. Appl.*, 2015, **4**, e356.
6 H. Zhang, D. Peng, W. Wang, L. Dong and C. Pan, *J. Phys. Chem. C*, 2015, **119**, 28136.
7 Y. Zhang, G. Gao, H. L. W. Chan, J. Dai, Y. Wang and J. Hao, *Adv. Mater.*, 2012, **24**, 1729.
8 M.-C. Wong, L. Chen, M.-K. Tsang, Y. Zhang and J. Hao, *Adv. Mater.*, 2015, **27**, 4488.
9 L.-B. Huang, G. Bai, M.-C. Wong, Z. Yang, W. Xu and J. Hao, *Adv. Mater.*, 2016, **28**, 2744.
10 T. Aitasalo, P. Dereń, J. Hölsä, H. Jungner, J. C. Krupa, M. Lastusaari, J. Legendziewicz, J. Niittykoski and W. Stręk, *J. Solid State Chem.*, 2003, **171**, 114.
11 T. Matsuzawa, Y. Aoki, N. Takeuchi and Y. Murayama, *J. Electrochem. Soc.*, 1996, **143**, 2670.
12 K. Van den Eeckhout, P. F. Smet and D. Poelman, *Materials*, 2010, **3**, 2536.
13 K. Van den Eeckhout, D. Poelman and P. Smet, *Materials*, 2013, **6**, 2789.
14 Z. Pan, Y.-Y. Lu and F. Liu, *Nat. Mater.*, 2012, **11**, 58.
15 T. Maldiney, *et al.*, *Nat. Mater.*, 2014, **13**, 418.

16 A. Abdukayum, J.-T. Chen, Q. Zhao and X.-P. Yan, *J. Am. Chem. Soc.*, 2013, **135**, 14125.
17 Z. Li, Y. Zhang, X. Wu, L. Huang, D. Li, W. Fan and G. Han, *J. Am. Chem. Soc.*, 2015, **137**, 5304.
18 D. C. Rodriguez Burbano, E. M. Rodriguez, P. Dorenbos, M. Bettinelli and J. A. Capobianco, *J. Mater. Chem. C*, 2014, **2**, 228.
19 D. C. Rodríguez Burbano, S. K. Sharma, P. Dorenbos, B. Viana and J. A. Capobianco, *Adv. Opt. Mater.*, 2015, **3**, 551.
20 G.-Y. Adachi and N. Imanaka, *Chem. Rev.*, 1998, **98**, 1479.
21 P. F. Smet, I. Moreels, Z. Hens and D. Poelman, *Materials*, 2010, **3**, 2834.
22 P. Gluchowski, W. Strek, M. Lastusaari and J. Holsa, *Phys. Chem. Chem. Phys.*, 2015, **17**, 17246.
23 T.-W. Kuo, W.-R. Liu and T.-M. Chen, *Opt. Express*, 2010, **18**, 8187.
24 F. Auzel, *Chem. Rev.*, 2004, **104**, 139.
25 L.-D. Sun, Y.-F. Wang and C.-H. Yan, *Acc. Chem. Res.*, 2014, **47**, 1001.
26 X. Liu, C.-H. Yan and J. A. Capobianco, *Chem. Soc. Rev.*, 2015, **44**, 1299.
27 L.-D. Sun, H. Dong, P.-Z. Zhang and C.-H. Yan, *Annu. Rev. Phys. Chem.*, 2015, **66**, 619.
28 H. Dong, L.-D. Sun and C.-H. Yan, *Chem. Soc. Rev.*, 2015, **44**, 1608.
29 Z.-J. Zhang, A. Feng, X.-Y. Chen and J.-T. Zhao, *J. Appl. Phys.*, 2013, **114**, 213518.
30 B. Huang, *Phys. Chem. Chem. Phys.*, 2016, **18**, 25946.
31 J. Hölsä, *Electrochem. Soc. Interface*, 2009, **18**, 42.
32 L. Li, K.-L. Wong, P. Li and M. Peng, *J. Mater. Chem. C*, 2016, **4**, 8166.
33 J.-C. Zhang, C.-N. Xu, S. Kamimura, Y. Terasawa, H. Yamada and X. Wang, *Opt. Express*, 2013, **21**, 12976.
34 J.-C. Zhang, L.-Z. Zhao, Y.-Z. Long, H.-D. Zhang, B. Sun, W.-P. Han, X. Yan and X. Wang, *Chem. Mater.*, 2015, **27**, 7481.
35 B. Huang, *Inorg. Chem.*, 2015, **54**, 11423.
36 B. Huang, *Phys. Chem. Chem. Phys.*, 2016, **18**, 13564.
37 B. Huang, R. Gillen and J. Robertson, *J. Phys. Chem. C*, 2014, **118**, 24248.
38 B. Huang, *Philos. Mag.*, 2014, **94**, 3052.
39 B. Huang and J. Robertson, *Phys. Rev. B: Condens. Matter Mater. Phys.*, 2012, **85**, 125305.
40 B. Huang and J. Robertson, *J. Non-Cryst. Solids*, 2012, **358**, 2393.
41 B. Huang, *Phys. Status Solidi B*, 2015, **252**, 431.
42 A. De Vos, K. Lejaeghere, D. E. P. Vanpoucke, J. J. Joos, P. F. Smet and K. Hemelsoet, *Inorg. Chem.*, 2016, **55**, 2402.
43 B. Qu, B. Zhang, L. Wang, R. Zhou and X. C. Zeng, *Chem. Mater.*, 2015, **27**, 2195.
44 C. J. Duan, A. C. A. Delsing and H. T. Hintzen, *Chem. Mater.*, 2009, **21**, 1010.
45 P. Li, S. Deng, L. Zhang, G. Liu and J. Yu, *Chem. Phys. Lett.*, 2012, **531**, 75.
46 S. J. Clark, J. Robertson, S. Lany and A. Zunger, *Phys. Rev. B: Condens. Matter Mater. Phys.*, 2010, **81**, 115311.
47 A. Janotti and C. G. Van de Walle, *Phys. Rev. B: Condens. Matter Mater. Phys.*, 2007, **76**, 165202.
48 S. J. Clark, M. D. Segall, C. J. Pickard, P. J. Hasnip, M. I. J. Probert, K. Refson and M. C. Payne, *Z. Kristallogr.*, 2005, **220**, 567.
49 N. Marzari, D. Vanderbilt and M. C. Payne, *Phys. Rev. Lett.*, 1997, **79**, 1337.
50 M. I. J. Probert and M. C. Payne, *Phys. Rev. B: Condens. Matter Mater. Phys.*, 2003, **67**, 075204.
51 I. A. Vladimir, F. Aryasetiawan and A. I. Lichtenstein, *J. Phys.: Condens. Matter*, 1997, **9**, 767.
52 C. J. Pickard, B. Winkler, R. K. Chen, M. C. Payne, M. H. Lee, J. S. Lin, J. A. White, V. Milman and D. Vanderbilt, *Phys. Rev. Lett.*, 2000, **85**, 5122.
53 B. Huang, *Solid State Commun.*, 2016, **230**, 49.
54 B. Huang, *Solid State Commun.*, 2016, **237–238**, 34.
55 B. Huang, *J. Comput. Chem.*, 2016, **37**, 825.
56 B. Huang, H. Dong, K.-L. Wong, L.-D. Sun and C.-H. Yan, *J. Phys. Chem. C*, 2016, **120**, 18858.
57 S. Lany and A. Zunger, *Phys. Rev. B: Condens. Matter Mater. Phys.*, 2009, **80**, 085202.
58 S. Lany and A. Zunger, *Phys. Rev. B: Condens. Matter Mater. Phys.*, 2010, **81**, 205209.
59 B. J. Morgan and G. W. Watson, *J. Phys. Chem. C*, 2010, **114**, 2321.
60 P. R. L. Keating, D. O. Scanlon, B. J. Morgan, N. M. Galea and G. W. Watson, *J. Phys. Chem. C*, 2011, **116**, 2443.
61 A. M. Rappe, K. M. Rabe, E. Kaxiras and J. D. Joannopoulos, *Phys. Rev. B: Condens. Matter Mater. Phys.*, 1990, **41**, 1227.
62 L. Kleinman and D. M. Bylander, *Phys. Rev. Lett.*, 1982, **48**, 1425.
63 S. G. Louie, S. Froyen and M. L. Cohen, *Phys. Rev. B: Condens. Matter Mater. Phys.*, 1982, **26**, 1738.
64 S. Lany and A. Zunger, *Phys. Rev. B: Condens. Matter Mater. Phys.*, 2008, **78**, 235104.
65 P. Tanner, in *Lanthanide Luminescence*, ed. P. Hänninen and H. Härmä, Springer, Berlin Heidelberg, 2011, vol. 7, p. 183.
66 S. Lany and A. Zunger, *Phys. Rev. Lett.*, 2004, **93**, 156404.
67 S. Lany and A. Zunger, *Phys. Rev. B: Condens. Matter Mater. Phys.*, 2005, **72**, 035215.
68 Z. Qiu, C. Rong, W. Zhou, J. Zhang, C. Li, L. Yu, S. Liu and S. Lian, *J. Alloys Compd.*, 2014, **583**, 335.

